

# Cosmology from clustering of Ly $\alpha$ galaxies: breaking non-gravitational Ly $\alpha$ radiative transfer degeneracies using the bispectrum

Bradley Greig,<sup>1,2\*</sup> Eiichiro Komatsu,<sup>3,4,5†</sup> & J. Stuart B. Wyithe;<sup>1,2‡</sup>

<sup>1</sup>*School of Physics, University of Melbourne, Parkville, Victoria 3010, Australia*

<sup>2</sup>*ARC Centre of Excellence for All-sky Astrophysics (CAASTRO)*

<sup>3</sup>*Texas Cosmology Center and the Department of Astronomy, The University of Texas at Austin, 1 University Station, C1400, Austin, TX 78712, USA*

<sup>4</sup>*Kavli Institute for the Physics and Mathematics of the Universe, Todai Institutes for Advanced Study, the University of Tokyo, Kashiwa, Japan 277-8583 (Kavli IPMU, WPI)*

<sup>5</sup>*Max-Planck-Institut für Astrophysik, Karl-Schwarzschild Str. 1, 85741 Garching, Germany*

22 October 2021

## ABSTRACT

Large surveys for Ly $\alpha$  emitting (LAE) galaxies have been proposed as a new method for measuring clustering of the galaxy population at high redshift with the goal of determining cosmological parameters. However, Ly $\alpha$  radiative transfer effects may modify the observed clustering of LAE galaxies in a way that mimics gravitational effects, potentially reducing the precision of cosmological constraints. For example, the effect of the linear redshift-space distortion on the power spectrum of LAE galaxies is potentially degenerate with Ly $\alpha$  radiative transfer effects owing to the dependence of observed flux on intergalactic medium velocity gradients. In this paper, we show that the three-point function (bispectrum) can distinguish between gravitational and non-gravitational effects, and thus breaks these degeneracies, making it possible to recover cosmological parameters from LAE galaxy surveys. Constraints on the angular diameter distance and the Hubble expansion rate can also be improved by combining power spectrum and bispectrum measurements.

**Key words:** galaxies: high-redshift - cosmology: theory - large-scale structure of universe

## 1 INTRODUCTION

For the past three decades galaxy redshift surveys have served as the traditional method for constraining cosmological parameters such as the matter density of the universe and the equation of state of dark energy, by measuring the clustering of galaxies. These have been restricted to  $z < 1$  due to the increasingly fainter galaxy magnitudes and larger required cosmic volumes, which render spectroscopy of large numbers of photometrically selected early type galaxies plausible only at such low redshifts. Recently the WiggleZ collaboration has pushed galaxy clustering work to  $z \sim 1$  using emission lines from star-forming galaxies (Blake et al. 2011a,b,c, 2012).

Ly $\alpha$  emitting (LAE) galaxies are detectable out to

high redshift (Iye et al. 2006; Kashikawa et al. 2006; Lehnert et al. 2010; Ouchi et al. 2010), due to their strong line emission. Indeed over the previous few years, the number of detected LAE sources has steadily grown and the sample sizes of LAE galaxies have reached sufficient size for clustering studies (Gawiser et al. 2007; Kovač et al. 2007; Orsi et al. 2008; Guaita et al. 2010; Ouchi et al. 2010).

While the existing samples of LAE galaxies are still too small for cosmological purposes, the rate of detection of these LAE galaxies will significantly improve with the upcoming Hobby-Eberly Telescope Dark Energy Experiment (HETDEX, Hill et al. 2004, 2008), whose aim is to spectroscopically measure the redshifts of 800 000 LAE galaxies in the redshift range  $1.9 \leq z \leq 3.5$  (Hill et al. 2004, 2008) with the total sky coverage of 420 square degrees and the total volume coverage of 10 Gpc<sup>3</sup>. This survey is specifically designed to use the clustering of LAE galaxies to make the precise measurement of the distance

\* E-mail: bgreig@student.unimelb.edu.au (BG)

† komatsu@mpa-garching.mpg.de (EK)

‡ swyithe@unimelb.edu.au (JSBW)

scales, both the angular diameter distance ( $D_A$ ) and the Hubble rate ( $H$ ), as a function of  $z$  out to  $z \sim 3$ .

In order for us to use the clustering of LAE galaxies to measure the distance scales, we must understand how the clustering of LAE galaxies is related to the underlying matter distribution. Simulations by Zheng et al. (2010, 2011) and Laursen et al. (2011) have investigated the radiative transfer effects on the Ly $\alpha$  emission of LAE galaxies both within the circumgalactic environment around the halo and from the resonant scattering of diffuse neutral hydrogen in the intergalactic medium (IGM). Of particular interest is the clustering of the LAE galaxies: Zheng et al. (2011) find that line-of-sight gradients in the peculiar velocity of LAE galaxies could lead to an observed reduction in the line-of-sight clustering amplitude of the galaxies, counteracting the strength of the typical Kaiser effect (Kaiser 1987) caused by gravitation. Conversely, the clustering of LAE galaxies transverse to the line-of-sight is found to be significantly boosted by the Ly $\alpha$  radiative transfer effects. In addition to the local effects of peculiar velocity gradients, the transmission of the Ly $\alpha$  emission line of LAE galaxies through the diffuse IGM could also be affected by fluctuations in the UV ionizing background and to changes in the neutral hydrogen fraction associated with changes in the density around the local environment.

To understand these effects, Zheng et al. (2011) and Wyithe & Dijkstra (2011) have derived analytic models to describe the observed modifications of the power spectrum of LAE galaxies. Both derive quantities that directly relate to the non-gravitational effects expected from the Ly $\alpha$  radiative effects. Wyithe & Dijkstra (2011) use this model to study the expected recovery of both cosmological and Ly $\alpha$  radiative transfer parameters from a survey corresponding to HETDEX. They find that some cosmological parameters derived only from the power spectrum are degenerate with the Ly $\alpha$  radiative transfer effects, and that this has direct consequences for the accuracy with which cosmological parameters can be recovered from the LAE galaxy power spectrum. Prior knowledge of the magnitude of the radiative transfer effects can improve the recovery of the cosmological constraints.

In this paper we further investigate the effects of non-gravitational LAE clustering on the recovery of cosmological parameters. We extend and improve the linear theory work of Wyithe & Dijkstra (2011) by including the three-point correlation function (bispectrum) and by combining with the power spectrum, to break the first order degeneracies of the Ly $\alpha$  radiative transfer effects and cosmological parameters. To calculate the bispectrum, we use a next-to-leading order Eulerian perturbation theory approach (Bernardeau et al. 2002 and references within), and derive expressions valid into the mildly non-linear regime. We also derive higher-order expressions for the Ly $\alpha$  radiative transfer effects, including the higher-order effects of redshift-space distortions. We then study how well a joint analysis of the power spectrum and the bispectrum can break the cosmological and radiative transfer degeneracies. We provide the expected constraints on cosmological parameters through the application of Fisher matrices, with specific reference to the HETDEX survey.

This paper is set out as follows. In Section 2 we outline the degeneracies between cosmological and Ly $\alpha$  radiative transfer parameters, and in Section 3 perform a Fisher matrix analysis of the LAE galaxy power spectrum. In Section 4 we outline and describe existing Eulerian perturbation theory expressions and provide the derivation of higher-order corrections for the Ly $\alpha$  radiative transfer effects, in order to construct both a bispectrum and a reduced bispectrum model. In Sections 5 and 6 we perform Fisher matrix analyses of the reduced bispectrum alone, and a combined power spectrum and bispectrum in order to provide cosmological parameter estimates. We finish with our summary and final remarks in Section 7. In our numerical calculations we consider the standard set of cosmological parameters (Komatsu et al. 2011), with  $\Omega_m = 0.275$ ,  $\Omega_\Lambda = 0.725$ ,  $\Omega_b = 0.0458$ ,  $n_s = 0.968$ ,  $h = 0.702$  and  $\sigma_8 = 0.816$ .

## 2 CLUSTERING OF Ly $\alpha$ EMITTERS

In this section we summarize the linear theory clustering of LAE galaxies. For a galaxy redshift survey, one can write a simple expression relating the power spectrum of galaxies to the underlying matter distribution. However, for LAE galaxies, Zheng et al. (2011) and Wyithe & Dijkstra (2011) show that Ly $\alpha$  radiative transfer effects modify this relationship.

### 2.1 Galaxy power spectrum

In linear theory, the power spectrum of galaxies in redshift space is given by

$$P_{\text{gal}}(k) = (b_1 + f\mu^2)^2 P_L(k), \quad (1)$$

where  $b_1$  is the linear galaxy bias, since galaxies are biased tracers of the matter density field (Kaiser 1984),  $f \equiv \text{dln } D(a)/\text{dln } a$  is the growth rate of structure,  $D(a)$  is the linear growth factor,  $P_L(k)$  is the power spectrum of the linear density fluctuations, and  $\mu$  is the cosine of the angle between the line-of-sight vector  $\hat{z}$  and the wavevector  $\mathbf{k}$ , i.e.,  $\mu \equiv \mathbf{k} \cdot \hat{z}/k$ .

Of particular interest for cosmology is the recovery of the growth rate of structure,  $f$ , which can be parametrized as  $f = \Omega_m^\gamma$ . The value that  $\gamma$  takes can distinguish between cosmological models described by general relativity or other gravitational descriptions (Linder 2005). However, the galaxy bias,  $b_1$ , and the growth rate of structure,  $f$ , are degenerate in the above model. Hence, what is actually measurable from a galaxy redshift survey is the linear redshift-space distortion parameter,  $\beta = f/b_1$ . With this parameter, the above expression becomes

$$P_{\text{gal}}(k) = b_1^2 (1 + \beta\mu^2)^2 P_L(k). \quad (2)$$

### 2.2 LAE power spectrum

Ly $\alpha$  radiative transfer effects potentially modify the power spectrum of LAE galaxies away from the standard galaxy description (Equation 1). This arises because the

observed number density of Ly $\alpha$  galaxies at a fixed observed flux depends on how many Ly $\alpha$  photons escape to observers. Thus the observed density of galaxies can be modified by the local environment nearby to the Ly $\alpha$  galaxies.

The Ly $\alpha$  optical depth through the IGM depends on the local density ( $\rho$ ), the ionizing background strength ( $\Gamma$ ), and also on the strength of the local peculiar velocity gradient along the line-of-sight ( $dv_z/dr$ ),

$$\tau \propto \frac{\rho^2}{\Gamma T^{0.7} \frac{dv_z}{dr}} \propto \frac{\rho^{2-0.7(\gamma-1)}}{\Gamma \frac{dv_z}{dr}}, \quad (3)$$

where  $\gamma$  is the polytropic index, used to relate the temperature to the underlying density field as  $T \propto \rho^{\gamma-1}$  with  $\gamma = 1.4$  (Hui & Gnedin 1997).

In this section we shall describe the effect of Ly $\alpha$  transmission fluctuations on the observed clustering signal of LAEs, following Wyithe & Dijkstra (2011). Modifications to the intrinsic Ly $\alpha$  luminosity by the IGM induce a change in number counts of LAE galaxies. The number density of LAE sources,  $n_{\text{Ly}\alpha}$ , that are observed above some observational flux threshold,  $F_0$ , can be expressed relative to the average,  $\bar{n}_{\text{Ly}\alpha}(> L_0, \rho_0, \Gamma_0, \delta(\mathbf{x}))$ , as

$$n_{\text{Ly}\alpha}(> F_0) = \bar{n}_{\text{Ly}\alpha}(> L_0, \rho_0, \Gamma_0, \delta(\mathbf{x})) \times [1 + \delta_g(\mathbf{x})], \quad (4)$$

where  $\delta(\mathbf{x})$  is the large-scale matter-density perturbation, and  $\delta_g(\mathbf{x})$  is the perturbation in the galaxy number density. Now the average number density of LAE galaxies depends on the fluctuations due to the non-gravitational Ly $\alpha$  radiative transfer effects; namely, the local density in the LAE environment,  $\rho$ , ionizing background,  $\Gamma$ , and peculiar velocity gradients,  $dv_z/dr$ .

We first obtain the expression for the mean number density of observed LAE galaxies. Taylor expanding about the three radiative transfer effects, we obtain

$$\bar{n}_{\text{Ly}\alpha}(> L_0, \rho_0, \Gamma_0, \delta(\mathbf{x})) = \bar{n}_{\text{Ly}\alpha}^{(0)} \left( 1 + \bar{n}_{\text{Ly}\alpha}^{(1)} \right), \quad (5)$$

where  $\bar{n}_{\text{Ly}\alpha}^{(0)}$  is just the mean number of LAE galaxies, and  $\bar{n}_{\text{Ly}\alpha}^{(1)}$  is the first-order Taylor-expanded expression evaluated around their mean quantity,

$$\begin{aligned} \bar{n}_{\text{Ly}\alpha}^{(1)} = & \frac{1}{\bar{n}_{\text{Ly}\alpha}^{(0)}} (\Gamma - \Gamma_0) \left. \frac{\partial \bar{n}_{\text{Ly}\alpha}}{\partial \Gamma} \right|_{F_0, \Gamma_0} + (\rho - \rho_0) \left. \frac{\partial \bar{n}_{\text{Ly}\alpha}}{\partial \rho} \right|_{F_0, \rho_0} \\ & + \left( \frac{dv_z}{d(ar_{\text{com}})} - H \right) \left. \frac{\partial \bar{n}_{\text{Ly}\alpha}}{\partial \frac{dv_z}{d(ar_{\text{com}})}} \right|_{F_0, \rho_0}. \end{aligned} \quad (6)$$

Here,  $H$  is the Hubble rate, and the line-of-sight velocity gradient is taken with respect to the comoving distance,  $r_{\text{com}}$ . We rewrite this expression for  $\bar{n}_{\text{Ly}\alpha}^{(1)}$  as

$$\bar{n}_{\text{Ly}\alpha}^{(1)} = \delta_\Gamma(\mathbf{x})C_\Gamma + \delta_\rho(\mathbf{x})C_\rho + \delta_v(\mathbf{x})C_v. \quad (7)$$

The constants  $C_\Gamma$ ,  $C_\rho$ , and  $C_v$ , are defined in Appendix A, and capture the distinct physical effects caused by changes to the local environment corresponding to either changes to the ionizing background, the density, or the velocity gradient along the line-of-sight, respectively. The other quantities are defined as  $\delta_\Gamma \equiv (\Gamma - \Gamma_0)/\Gamma_0$ ,  $\delta_\rho \equiv (\rho - \rho_0)/\rho_0$ , and  $\delta_v \equiv (Ha)^{-1} dv_z/dr_{\text{com}}$ .

Next, the number density of LAE galaxies observed

above a flux limit can be written as,

$$n_{\text{Ly}\alpha}(> F_0) = \bar{n}_{\text{Ly}\alpha}^{(0)} [1 + \delta_g(\mathbf{x})] \left[ 1 + \bar{n}_{\text{Ly}\alpha}^{(1)} \right], \quad (8)$$

where we have substituted Equation 5 into Equation 4. Rewriting this expression as fluctuations in the number of LAE galaxies relative to the mean number of galaxies expected without Ly $\alpha$  radiative transfer effects,  $\bar{n}_{\text{Ly}\alpha}^{(0)}$ , we obtain

$$\delta_{\text{Ly}\alpha}(\mathbf{x}) = \frac{n_{\text{Ly}\alpha}(> F_0)}{\bar{n}_{\text{Ly}\alpha}^{(0)}} - 1 = [1 + \delta_g(\mathbf{x})] \left[ 1 + \bar{n}_{\text{Ly}\alpha}^{(1)} \right] - 1. \quad (9)$$

Expanding Equation 9 and taking the Fourier transform, one finds, to the first order,

$$\delta_{\text{Ly}\alpha, s}(\mathbf{k}) = [b_1(1 + C_\Gamma) + C_\rho + f\mu^2(1 - C_v)] \delta(\mathbf{k}), \quad (10)$$

where we have used the linear-theory predictions:  $\delta_\Gamma(\mathbf{k}) = b_1 C_\Gamma \delta(\mathbf{k})$ ,  $\delta_\rho(\mathbf{k}) = \delta(\mathbf{k})$ , and  $\delta_v(\mathbf{k}) = -f\mu^2 C_v \delta(\mathbf{k})$ . Here, we have implicitly performed the linear redshift-space transformation (see Appendix B).

In this work we define the redshift-space LAE galaxy power spectrum as

$$\langle \delta_{\text{Ly}\alpha, s}(\mathbf{k}_1) \delta_{\text{Ly}\alpha, s}(\mathbf{k}_2) \rangle = (2\pi)^3 P_{\text{Ly}\alpha, s}(k) \delta^D(\mathbf{k}_1 + \mathbf{k}_2), \quad (11)$$

where  $P_{\text{Ly}\alpha, s}(k)$  is given by

$$P_{\text{Ly}\alpha, s}(k) = [b_1(1 + C_\Gamma) + C_\rho + f\mu^2(1 - C_v)]^2 P_L(k), \quad (12)$$

and  $P_L(k)$  is the linear real-space matter power spectrum. Relative to Equation 1, the addition of Ly $\alpha$  radiative transfer effects can lead to changes in the amplitude of the measured power spectrum.<sup>1</sup>

Equation 12 contains the main contributing terms of Zheng et al. (2011). However, we do not include the transverse line-of-sight velocity-gradient or the density-gradient (as provided by Zheng et al. 2011). As shown in Zheng et al. (2011), the effect of the density-gradient adds additional scale-dependant terms to the expression for the clustering of LAE galaxies on small scales. In this work, we are working at much larger scales, and so can ignore this scale-dependence and allow the density-gradient terms to be absorbed into the existing parameters of Equation 12.

The inclusion of Ly $\alpha$  radiative transfer effects introduces degeneracies between the cosmological parameters and Ly $\alpha$  radiative transfer parameters. In particular, from Equation 12, we note the degeneracy between the

<sup>1</sup> In Equation 12, we do not consider the scale dependence of the ionizing background fluctuations, which is the major difference between our expression and the expression in Wyithe & Dijkstra (2011). The ionizing background fluctuations are expected to be scale dependant, important on large scales (set by the mean free path of the ionizing photons) and becoming negligible on small scales. However, including the scale dependence associated with the ionizing background fluctuations increases the model complexity, providing additional model degeneracies. We feel that this simplification is justified since the transmission models investigated by Wyithe & Dijkstra (2011) find the magnitude of ionizing background fluctuations ( $C_\Gamma$ ) to be small compared to the other two radiative transfer effects. Hence, while ignoring the scale dependence is a simplification, the overall impact of removing this scale dependence should be minor.

growth rate of structure,  $f$ , and the line-of-sight peculiar velocity radiative transfer effect,  $C_v$ . Additionally, the galaxy bias,  $b_1$ , is degenerate with the local environment density,  $C_\rho$ , and the fluctuations in the ionizing background,  $C_\Gamma$ .

To simplify the expression, consider the following re-definition of Equation 12,

$$P_{\text{Ly}\alpha,s}(k) = \tilde{b}_1^2 \left[ 1 + \tilde{\beta} \mu^2 (1 - C_v) \right]^2 P_L(k), \quad (13)$$

where

$$\tilde{b}_1 \equiv b_1 + C_\rho + b_1 C_\Gamma. \quad (14)$$

This includes the large-scale effects of density and ionizing background which modify the observed galaxy clustering, and  $\tilde{\beta}$  which is a modified linear redshift-space distortion parameter corresponding to the modified galaxy bias,  $\tilde{\beta} \equiv f/\tilde{b}_1$ .

Now, the problem is clear: while Equation 13 has the same structure as Equation 2, the meaning of each parameter is different. The correspondence is  $b_1 \rightarrow \tilde{b}_1$  and  $\beta \rightarrow \tilde{\beta}(1 - C_v)$ , which shows the parameter degeneracy. In the next section we illustrate the resulting effect of radiative transfer parameters on the potential cosmological constraints.

### 3 COSMOLOGICAL CONSTRAINTS BASED ON THE LINEAR LAE GALAXY POWER SPECTRUM

To generate the expected constraints on cosmological parameters for a given survey configuration, we calculate the Fisher matrix which, for the galaxy power spectrum, can be written as (e.g., Seo & Eisenstein 2003)

$$F_{ij} = \int_0^{k_{\text{max}}} \frac{k^2 dk}{2\pi^2} \int_0^1 \frac{\partial \ln P_{\text{Ly}\alpha,s}}{\partial \theta_i} \frac{\partial \ln P_{\text{Ly}\alpha,s}}{\partial \theta_j} w(k, \mu) d\mu, \quad (15)$$

where  $w(k, \mu)$  is the weight given by

$$w(k, \mu) \equiv \frac{1}{2} \left[ \frac{n_g P_{\text{Ly}\alpha,s}(k, \mu)}{1 + n_g P_{\text{Ly}\alpha,s}(k, \mu)} \right]^2 V_{\text{survey}}. \quad (16)$$

Here,  $\theta_i$  is the parameter set of our  $i$ th dimensional model,  $n_g$  is the number density of LAE sources, and  $V_{\text{survey}}$  is the volume of the redshift survey.

We focus our attention on a survey like HETDEX, for which we assume the linear galaxy bias to be  $b_1 = 2.2$ . We generate constraints assuming measurement of one redshift bin at the midpoint of the HETDEX redshift range,  $z_{\text{min}} = 1.9$  and  $z_{\text{max}} = 3.5$ . At this redshift we have  $f = 0.972$  for the growth rate of structure. We assume HETDEX will detect 800 000 LAE galaxies in a total survey area of 420 sq. deg. We restrict our analysis to the weakly non-linear regime, selecting a maximum wavenumber,  $k_{\text{max}} = 0.3 h \text{ Mpc}^{-1}$ .

To generate the  $1-\sigma$  constraints for our cosmological parameters, we construct the one-dimensional maximum likelihood distribution from the Fisher matrix assuming a Gaussian distribution. The likelihood for the  $i$ th model

Parameter	Marginalization	PS 1- $\sigma$ (per cent)
$\beta$	$\ln(A)$	0.0091 (2.06)
$\beta$	$\ln(A), \ln(D_A), \ln(H)$	0.0213 (4.82)
$\ln(D_A)$	$\ln(A), \beta, \ln(H)$	0.0110 (1.10)
$\ln(H)$	$\ln(A), \beta, \ln(D_A)$	0.0132 (1.32)

**Table 1.** The  $1-\sigma$  constraints for the linear redshift-space distortion parameter,  $\beta$ , the angular diameter distance,  $\ln(D_A)$ , and the Hubble rate,  $\ln(H)$ , for a galaxy redshift survey with HETDEX-like survey parameters. The other model parameters are marginalized over, but no Ly $\alpha$  radiative transfer effects are included, i.e., the power spectrum is given by Equation 2.

parameter is

$$\mathcal{L}(\mathbf{x}_i) = \exp \left[ -\frac{1}{2} \bar{x}_i^2 \left( F_{ii} - \sum_{j,k \neq i}^{n-1} F_{ij} (\bar{F}_{jk})^{-1} F_{ki} \right) \right], \quad (17)$$

where  $\bar{x}_i \equiv (x_i - x_o)$  is defined to be the cosmological parameter value,  $x_i$ , subtracted by its fiducial value,  $x_o$ .  $F$  is the full Fisher matrix of the  $n$  parameter model, and  $\bar{F}$  the reduced Fisher matrix of the  $n-1$  parameter model with the  $i$ th row and column removed.

To generate the two-dimensional joint constraints on any two parameters, we use

$$\begin{aligned} \mathcal{L}(\mathbf{x}_i, \mathbf{x}_j) = \exp \left\{ -\frac{1}{2} \left[ \bar{x}_i^2 \left( F_{ii} - \sum_{k,l \neq i}^{n-2} F_{ik} (\bar{F}_{kl})^{-1} F_{li} \right) \right. \right. \\ \left. \left. + \bar{x}_j^2 \left( F_{jj} - \sum_{k,l \neq j}^{n-2} F_{jk} (\bar{F}_{kl})^{-1} F_{lj} \right) \right. \right. \\ \left. \left. + 2\bar{x}_i \bar{x}_j \left( F_{ij} - \sum_{k,l \neq i,j}^{n-2} F_{ik} (\bar{F}_{kl})^{-1} F_{lj} \right) \right] \right\}, \quad (18) \end{aligned}$$

which contains the cross term which determines the correlation between the two parameters being considered. Here,  $F$  is the full Fisher matrix of the  $n$  parameter model, and  $\bar{F}$  is the reduced Fisher matrix of the  $n-2$  parameter model, with the  $i$ th and  $j$ th rows and columns removed.

To investigate the degeneracies due to Ly $\alpha$  radiative transfer parameters, we consider recovery of cosmological parameters from three power spectra:

1. The galaxy power spectrum given by Equation 2,
2. A fiducial LAE power spectrum given by Equation 13 with the fiducial values of radiative transfer parameters set to vanish, i.e.,  $C_\Gamma = C_\rho = C_v = 0$  (but these radiative transfer parameters are marginalized over), and
3. A LAE power spectrum given by Equation 13 with the fiducial values of radiative transfer parameters set to some indicative values.

#### 3.1 Galaxy power spectrum

For the galaxy power spectrum given by Equation 2, the galaxy bias is completely degenerate with the amplitude

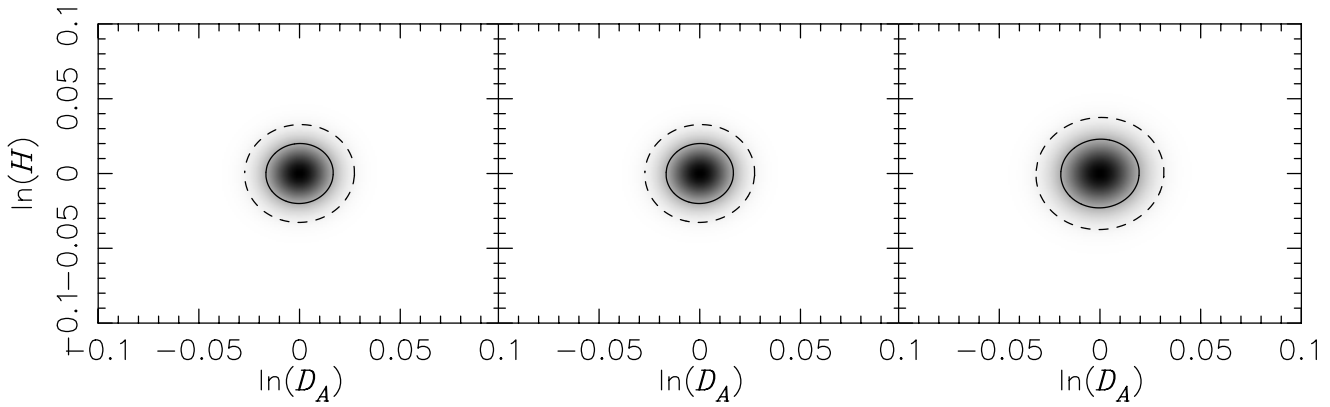


**Figure 1.** Two-dimensional marginalized joint distribution for the two cosmological distance scales: the angular diameter distance ( $D_A$ ) and the Hubble rate ( $H$ ). (*Left*) a typical galaxy redshift survey (no Ly $\alpha$  effects; no marginalization over  $C_v$ ), (*middle*) a fiducial LAE galaxy redshift survey (the fiducial values of the Ly $\alpha$  radiative transfer parameters set to vanish; marginalized over  $C_v$ ) and (*right*) a LAE galaxy redshift survey including the first-order Ly $\alpha$  radiative transfer effects given by  $C_\Gamma = 0.05$ ,  $C_\rho = -0.39$ , and  $C_v = 0.11$ . The error ellipse is slightly bigger for this case because the effective bias of LAE galaxies,  $\tilde{b}_1 = 1.9$ , is about 15% smaller than the fiducial value,  $b_1 = 2.2$ , reducing the amplitude of the power spectrum relative to the shot noise. The solid and dashed curves show the 1- and 2- $\sigma$  constraints generated from the likelihood distribution, respectively. Scale selected to aid comparison with Figure 7.

Parameter	Marginalization	No Priors on $C_v$ 1- $\sigma$ (per cent)	Perfect knowledge 1- $\sigma$ (per cent)	$\sigma_{C_v} = 0.01$ 1- $\sigma$ (per cent)	$\sigma_{C_v} = 0.1$ 1- $\sigma$ (per cent)	$\sigma_{C_v} = 0.5$ 1- $\sigma$ (per cent)
$\tilde{\beta}$	$\ln(A), C_v$	-	0.0091 (2.06)	0.0101 (2.29)	0.0451 (10.21)	0.2211 (50.04)
$\tilde{\beta}$	$\ln(A), \ln(D_A), \ln(H), C_v$	-	0.0213 (4.82)	0.0218 (4.93)	0.0491 (11.11)	0.2220 (50.24)
$\ln(D_A)$	$\ln(A), \tilde{\beta}, \ln(H), C_v$	0.0110 (1.10)	0.0110 (1.10)	0.0110 (1.10)	0.0110 (1.10)	0.0110 (1.10)
$\ln(H)$	$\ln(A), \tilde{\beta}, \ln(D_A), C_v$	0.0132 (1.32)	0.0132 (1.32)	0.0132 (1.32)	0.0132 (1.32)	0.0132 (1.32)

**Table 2.** The 1- $\sigma$  constraints for  $\tilde{\beta}$ ,  $\ln(D_A)$ , and  $\ln(H)$  for our fiducial LAE galaxy redshift survey (the fiducial values of the Ly $\alpha$  radiative transfer parameters set to vanish) marginalized over remaining model parameters shown in the second column. We compare varying priors added to the radiative transfer parameter,  $C_v$ , which suffers from a large degeneracy with  $\tilde{\beta}$ . The power spectrum model is given by Equation 13.

of the power spectrum ( $\sigma_8$ ). Furthermore, one cannot directly measure the growth rate of structure,  $f$ , but only the parameter  $\beta$ . We show later that by considering the bispectrum, one can directly probe  $f$ .

The cosmological parameters we determine from this model are therefore the overall amplitude [ $\ln(A)$ ], the linear redshift-space distortion parameter [ $\beta$ ], and the two distance measurements given by the angular diameter distance [ $\ln(D_A)$ ] and the Hubble rate [ $\ln(H)$ ]. The information on the galaxy bias is factored into the linear redshift-space distortion parameter and we redefine the amplitude to include galaxy bias. The constraints for  $\beta$  as well as  $\ln(D_A)$  and  $\ln(H)$  represent the best case scenario for how accurately we can recover the cosmological parameters from a galaxy power spectrum analysis.

In Table 1, we provide the 1- $\sigma$  constraints on  $\beta$ , and the two distance scales,  $D_A$  and  $H$ . For a galaxy redshift survey with HETDEX-like survey parameters, the expected uncertainty on the linear redshift-space distortion,  $\beta$ , is 0.021 (4.8 per cent), on the angular diameter distance it is 1.1 per cent, and on the Hubble rate it is 1.3 per cent. Our distance constraints for the above model are consistent with the results of Shoji et al. (2009).

Of particular interest for cosmological analyses is the two-dimensional joint constraints on the two distance measures,  $\ln(D_A)$  and  $\ln(H)$ . In the left panel of Figure

1, we show the 1- $\sigma$  and 2- $\sigma$  joint constraints on  $\ln(D_A)$  and  $\ln(H)$ , which give the baseline for comparison with the recovery of the cosmological distance parameters for  $D_A$  and  $H$  for the remainder of this work.

### 3.2 Fiducial LAE galaxy power spectrum

We model the LAE galaxy power spectrum using Equation 13. In our fiducial case, we set all Ly $\alpha$  radiative transfer coefficients to zero, i.e.,  $\tilde{b}_1 = b_1$ ,  $\tilde{\beta} = \beta$ , and  $C_v = 0$ . Although we set the Ly $\alpha$  radiative transfer effects to zero, we still marginalize over the possible existence of  $C_v$  in this case.

The amplitude of the power spectrum is completely degenerate with the modified galaxy bias, and so we can redefine the amplitude to include  $\tilde{b}_1$ . The LAE galaxy power spectrum includes  $C_v$ , the Ly $\alpha$  radiative transfer effect associated with the line-of-sight peculiar velocity gradient. Hence, for the LAE galaxy power spectrum, the model contains 5 parameters,  $\ln(A)$ ,  $\tilde{\beta}$ ,  $C_v$ ,  $\ln(D_A)$ , and  $\ln(H)$ . The linear redshift-space distortion parameter,  $\tilde{\beta}$ , and the radiative transfer effect,  $C_v$ , are completely degenerate; however, with the addition of priors on  $C_v$ , one can break the degeneracy and improve the constraints on the linear distortion parameter,  $\tilde{\beta}$  (Wyithe & Dijkstra 2011).

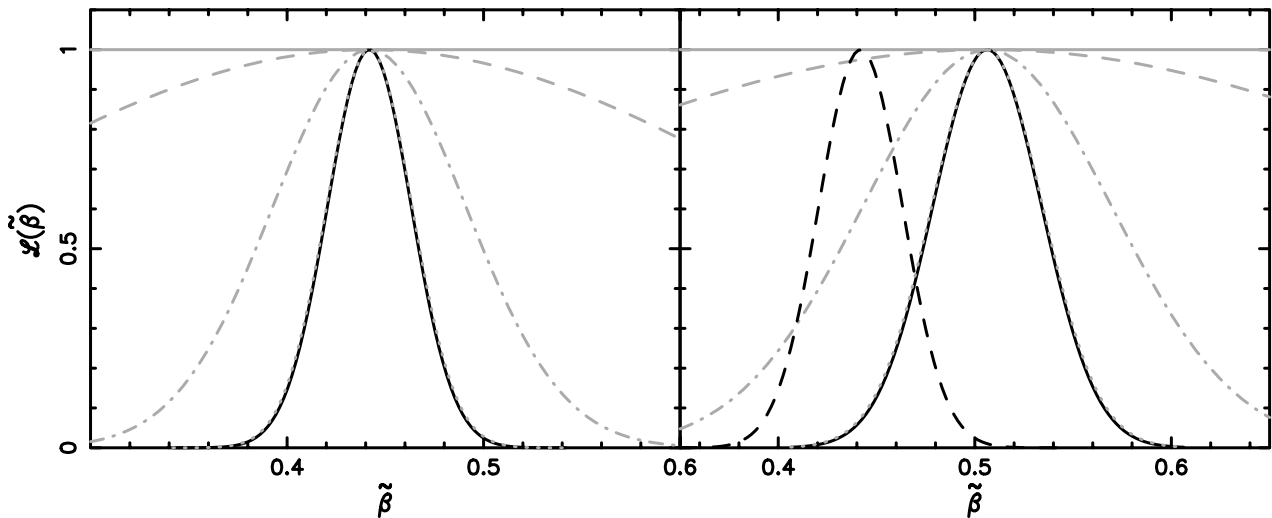


**Figure 2.** One-dimensional marginalized likelihood distributions for the linear redshift-space distortion parameter ( $\tilde{\beta}$ ) generated from; (*left*) the fiducial LAE galaxy power spectrum (no Ly $\alpha$  effects, but marginalized over  $C_v$ ), and (*right*) a LAE galaxy power spectrum including Ly $\alpha$  radiative transfer effects ( $C_\Gamma = 0.05$ ,  $C_\rho = -0.39$ , and  $C_v = 0.11$ ). The resultant offset in  $\tilde{\beta}$  in the LAE galaxy power spectrum (*right panel*) is due to the modified bias because of the included Ly $\alpha$  radiative transfer effects. The various curves denote different priors added to  $C_v$  and are as follows, *black solid*: perfect knowledge ( $\sigma_{C_v} = 0.0001$ ), *grey dotted*:  $\sigma_{C_v} = 0.01$ , *grey dot-dashed*:  $\sigma_{C_v} = 0.1$ , *grey dashed*:  $\sigma_{C_v} = 0.5$ , and *grey solid*: no priors added. In the right panel, the *black dashed* offset curve is the comparison to the case corresponding to perfect knowledge on  $C_v$  from the fiducial LAE galaxy power spectrum (*black solid curve, left panel*).

Parameter	Marginalization	No Priors on $C_v$ 1- $\sigma$ (per cent)	Perfect knowledge 1- $\sigma$ (per cent)	$\sigma_{C_v} = 0.01$ 1- $\sigma$ (per cent)	$\sigma_{C_v} = 0.1$ 1- $\sigma$ (per cent)	$\sigma_{C_v} = 0.5$ 1- $\sigma$ (per cent)
$\tilde{\beta}$	$\ln(A), C_v$	-	0.0121 (2.39)	0.0134 (2.65)	0.0582 (11.49)	0.2847 (56.23)
$\tilde{\beta}$	$\ln(A), \ln(D_A), \ln(H), C_v$	-	0.0278 (5.49)	0.0283 (5.59)	0.0633 (12.50)	0.2858 (56.45)
$\ln(D_A)$	$\ln(A), \tilde{\beta}, \ln(H), C_v$	0.0128 (1.28)	0.0128 (1.28)	0.0128 (1.28)	0.0128 (1.28)	0.0128 (1.28)
$\ln(H)$	$\ln(A), \tilde{\beta}, \ln(D_A), C_v$	0.0151 (1.51)	0.0151 (1.51)	0.0151 (1.51)	0.0151 (1.51)	0.0151 (1.51)

**Table 3.** Same as Table 1, but for the LAE galaxy redshift survey including first order Ly $\alpha$  radiative transfer effects,  $C_\Gamma = 0.05$ ,  $C_\rho = -0.39$  and  $C_v = 0.11$ .

In Table 2, we provide the resulting 1- $\sigma$  constraints on the linear redshift-space distortion parameter,  $\tilde{\beta}$ , as well as the distance constraints, marginalized over the remaining model parameters including  $C_v$ . The columns from left to right in Table 2 consider priors added to  $C_v$ ; essentially perfect knowledge of  $C_v$ ,  $\sigma_{C_v} = 0.0001^2$ ,  $\sigma_{C_v} = 0.01$ ,  $\sigma_{C_v} = 0.1$ , and  $\sigma_{C_v} = 0.5$ . The inclusion of  $C_v$  into the model significantly impacts the recovery of the linear redshift-space distortion parameter,  $\tilde{\beta}$ , whereas the distance constraints remain unaffected by the marginalization over the radiative transfer effects. This differs from Wyithe & Dijkstra (2011) where inclusion of scale-dependent ionizing background fluctuations lead to reduced distance constraints.

With sufficiently tight priors on  $C_v$ , the constraints on  $\tilde{\beta}$  approach the results given in the previous section, as expected. If we have a poor understanding of  $C_v$ , however, the ability to recover  $\tilde{\beta}$  drops by an order of mag-

nitude. See the left panel of Figure 2 for a graphical representation of the effect of the priors.

On the other hand, the distance constraints are unaffected by the degeneracy between  $\tilde{\beta}$  and  $C_v$ . (Compare the middle panel of Figure 1 with the left panel.) This is because  $\beta$  and  $C_v$  enter into the power spectrum in the same way: as far as the distance scales are concerned, it makes no difference whether one marginalizes over  $\beta$  in Equation 2 or  $\tilde{\beta}(1 - C_v)$  in Equation 13.

### 3.3 LAE galaxy power spectrum

Wyithe & Dijkstra (2011) show that the magnitude of the Ly $\alpha$  radiative transfer parameters varies significantly depending on the LAE model considered. In particular the magnitude of the effect is significantly larger in the absence of a galactic outflow, so that the absorption is dominated by infalling IGM. For illustration we consider this ‘infall’ model with an escape fraction of 10 per cent, as this is the model with the largest magnitude Ly $\alpha$  radiative transfer effects. Hence, when we include the radiative transfer effects into our model, we set  $C_\Gamma = 0.05$ ,  $C_\rho = -0.39$ , and  $C_v = 0.11$  in Equation 13.

<sup>2</sup> Throughout this work we define the ‘perfect knowledge on  $C_v$ ’ as a prior set to  $\sigma_{C_v} = 0.0001$ , which is to ensure that our Fisher matrix elements remain finite, yet still mimic the behaviour for perfectly understood parameters.

In Table 3, we provide estimates for the recovery of cosmological parameters when we include the radiative transfer effects. The linear bias is modified from its fiducial value of  $b_1 = 2.2$  to  $\tilde{b}_1 = 1.9$ , acting to reduce the observed clustering of LAE galaxies. As the level of the shot noise is the same, a reduced effective bias implies a lower signal-to-noise for measuring the power spectrum of LAE galaxies. As a result, the expected constraints on the angular diameter distance and the Hubble rate are worse than the previous two cases. One can see this clearly in the right panel of Figure 1.

The same is true for  $\tilde{\beta}$ : due to a smaller effective bias, the fractional precision by which we can determine  $\tilde{\beta}$  is slightly worse than the previous cases. (One can see this by comparing the rows of ‘ $\beta$ ’ in Table 2 and 3.) Note also that, as the fiducial value of  $\tilde{b}_1$  is different due to the radiative transfer parameters, the fiducial value of  $\tilde{\beta} = f/\tilde{b}_1$  is also different.

In Figure 2, we show the one-dimensional likelihood distributions for  $\tilde{\beta}$  for both the fiducial LAE galaxy model (left panel) and the LAE galaxy model (with Ly $\alpha$  effects, right panel). As already described in the previous section, the recovery of  $\tilde{\beta}$  from these models is highly sensitive to the priors on  $C_v$ , with marginal improvement on the priors breaking the degeneracy between  $\tilde{\beta}$  and  $C_v$ . In the right panel, we compare the likelihood distribution for the case of perfect knowledge of  $C_v$  for the fiducial LAE galaxy model (the dashed line) to the LAE galaxy model (the solid line), showing the degree of offset that the Ly $\alpha$  radiative transfer parameters have on the fiducial value of  $\tilde{\beta}$ .

Thus inclusion of the Ly $\alpha$  radiative transfer parameters impacts the recovery of cosmological constraints, most notably the growth rate of structure  $f$  through the recovery of the linear redshift-space distortion parameter  $\tilde{\beta}$ . Unless we have a good prior knowledge on the value of  $C_v$ , it seems hopeless to determine  $\tilde{\beta}$  with any precision. Fortunately, one can break the degeneracy between  $\tilde{\beta}$  and  $C_v$  by including the three-point function (bispectrum), as we shall show next.

#### 4 BISPECTRUM AND NON-LINEAR CLUSTERING OF LAE GALAXIES

If primordial perturbations are Gaussian, linear density fields are also Gaussian, in which case the bispectrum of linear density fields vanishes. The bispectrum is defined as

$$\langle \delta(\mathbf{k}_1)\delta(\mathbf{k}_2)\delta(\mathbf{k}_3) \rangle = (2\pi)^3 B(\mathbf{k}_1, \mathbf{k}_2, \mathbf{k}_3)\delta^D(\mathbf{k}_1 + \mathbf{k}_2 + \mathbf{k}_3). \quad (19)$$

However, non-linear gravitational evolution of density fields, and non-linear gravitational and non-gravitational evolution of galaxy bias make the observed galaxy density fields non-Gaussian. As a result, the observed bispectrum does not vanish, providing information regarding non-linear evolution of density fields.

In the previous section, we have considered the linear-theory power spectrum model for the LAE galaxy population. Structure formation is inherently a non-linear process, and by considering the true non-linear galaxy

power spectrum one would expect to increase the constraining power. However, the non-linear power spectrum alone will not achieve this, due to the additional parameters required to fully describe it. Hence the simple linear LAE galaxy power spectrum is preferred instead of the increased model complexity provided by the non-linear LAE galaxy power spectrum. On the other hand additional information on large scales may be contained in the non-Gaussianity associated with structure formation.

We use this information to break the degeneracy between cosmological parameters and Ly $\alpha$  radiative transfer parameters. There are three effects: (1) gravitational evolution of matter density fields, (2) gravitational and non-gravitational evolution of galaxy formation (captured by galaxy bias), and (3) non-gravitational Ly $\alpha$  radiative transfer effects.

#### 4.1 Eulerian perturbation theory

First, we summarize the non-linear gravitational evolution of density fields. Specifically, we apply standard Eulerian perturbation theory (Bernardeau et al. 2002 and references within) which, at larger redshifts, has been shown to describe the power spectrum measured from N-body simulations accurately (Jeong & Komatsu 2006).

The next-to-leading order corrections to the matter density field,  $\delta$ , as well as to the velocity-divergence field,  $\eta$ , are generated from the following expressions:

$$\begin{aligned} \delta(\mathbf{k}, z) &= \sum_{n=1}^{\infty} D^n(z) \int \frac{d^3 \mathbf{q}_1}{(2\pi)^3} \int \frac{d^3 \mathbf{q}_{n-1}}{(2\pi)^3} \\ &\times \int d^3 \mathbf{q}_n \delta^D(\mathbf{k} - \sum_{i=1}^n \mathbf{q}_i) F_n^{(s)}(\mathbf{q}_1, \mathbf{q}_2, \dots, \mathbf{q}_n) \\ &\times \delta_1(\mathbf{q}_1)\delta_1(\mathbf{q}_2)\dots\delta_1(\mathbf{q}_n) \end{aligned} \quad (20)$$

$$\begin{aligned} \eta(\mathbf{k}, z) &= \sum_{n=1}^{\infty} D^n(z) \int \frac{d^3 \mathbf{q}_1}{(2\pi)^3} \int \frac{d^3 \mathbf{q}_{n-1}}{(2\pi)^3} \\ &\times \int d^3 \mathbf{q}_n \delta^D(\mathbf{k} - \sum_{i=1}^n \mathbf{q}_i) G_n^{(s)}(\mathbf{q}_1, \mathbf{q}_2, \dots, \mathbf{q}_n) \\ &\times \delta_1(\mathbf{q}_1)\delta_1(\mathbf{q}_2)\dots\delta_1(\mathbf{q}_n), \end{aligned} \quad (21)$$

where  $D(z)$  is the linear growth factor describing the evolution of the linear density field,  $\delta_1(\mathbf{q}_i)$ , which is a Gaussian random field, and  $F_n^{(s)}$  and  $G_n^{(s)}$  are symmetrized kernel expressions generated from recursive relations (Jain & Bertschinger 1994). We deal only with the next-to-leading order expressions, for which the kernels are well known:

$$F_2^{(s)}(\mathbf{q}_1, \mathbf{q}_2) = \frac{5}{7} + \frac{2}{7} \frac{(\mathbf{q}_1 \cdot \mathbf{q}_2)^2}{q_1^2 q_2^2} + \frac{\mathbf{q}_1 \cdot \mathbf{q}_2}{2} \left( \frac{1}{q_1^2} + \frac{1}{q_2^2} \right), \quad (22)$$

$$G_2^{(s)}(\mathbf{q}_1, \mathbf{q}_2) = \frac{3}{7} + \frac{4}{7} \frac{(\mathbf{q}_1 \cdot \mathbf{q}_2)^2}{q_1^2 q_2^2} + \frac{\mathbf{q}_1 \cdot \mathbf{q}_2}{2} \left( \frac{1}{q_1^2} + \frac{1}{q_2^2} \right). \quad (23)$$

#### 4.2 Galaxy bias

Galaxies are biased tracers of the underlying dark matter density field (Kaiser 1984). Pushing into the weakly non-linear regime, we anticipate contributions from both the

linear and non-linear mapping of galaxies to the dark matter field.

The bias of galaxies differs from population to population, and their exact value depends on the underlying galaxy formation processes. Typically we expect a scale-dependant bias relating the clustering of the galaxies to the underlying matter density on small scales, but on large scales we expect the bias to be scale-independent.

To estimate the clustering of galaxies, we Taylor-expand the fluctuations in the number density of galaxies,  $\delta_g(\mathbf{x})$ , in terms of the underlying matter density field fluctuations (Fry & Gaztanaga 1993; McDonald 2006):

$$\delta_g(\mathbf{x}) = \epsilon(\mathbf{x}) + b_1\delta(\mathbf{x}) + \frac{1}{2}b_2\delta(\mathbf{x})^2 + \dots, \quad (24)$$

where  $\delta(\mathbf{x})$  is the non-linear matter density field, and  $b_1$  and  $b_2$  are the linear and non-linear bias parameters, respectively. The  $\epsilon(\mathbf{x})$  term is a stochasticity parameter describing the non-deterministic relationship between galaxies and the underlying matter distribution (Yoshikawa et al. 2001). We shall assume that  $\epsilon$  is a Gaussian field which is not correlated with  $\delta$ , i.e.,  $\langle \epsilon^3 \rangle = 0$  and  $\langle \epsilon\delta \rangle = 0$ . Under this assumption,  $\epsilon$  does not contribute to the bispectrum, and thus we shall ignore stochasticity throughout this paper.

### 4.3 LAE kernel expressions

In Section 2.2, we outline the derivation for the first-order Ly $\alpha$  radiative transfer effects. To derive higher-order expressions for the Ly $\alpha$  radiative transfer effects, we Taylor-expand  $n_{\text{Ly}\alpha}(> F_0)$  about the three non-gravitational Ly $\alpha$  radiative transfer effects, in analogy to the galaxy bias derivation (Fry & Gaztanaga 1993). We obtain

$$\bar{n}_{\text{Ly}\alpha}(> L_0, \rho_0, \Gamma_0, \delta(\mathbf{x})) = \bar{n}_{\text{Ly}\alpha}^{(0)} \left( 1 + \bar{n}_{\text{Ly}\alpha}^{(1)} + \bar{n}_{\text{Ly}\alpha}^{(2)} \right), \quad (25)$$

where  $\bar{n}_{\text{Ly}\alpha}^{(1)}$  and  $\bar{n}_{\text{Ly}\alpha}^{(2)}$  are the first- and second-order Taylor-expanded expressions, respectively, evaluated around the mean quantity  $\bar{n}_{\text{Ly}\alpha}^{(0)}$ . The term  $\bar{n}_{\text{Ly}\alpha}^{(1)}$  is given in Equation 6, and  $\bar{n}_{\text{Ly}\alpha}^{(2)}$  is given by

$$\begin{aligned} \bar{n}_{\text{Ly}\alpha}^{(2)} = & \frac{1}{2} \frac{1}{\bar{n}_{\text{Ly}\alpha}^{(0)}} \left[ \left( \Gamma - \Gamma_0 \right) \frac{\partial}{\partial \Gamma} \Big|_{F_0, \Gamma_0} + (\rho - \rho_0) \frac{\partial}{\partial \rho} \Big|_{F_0, \rho_0} \right. \\ & \left. + \left( \frac{dv_z}{d(ar_{\text{com}})} - H \right) \frac{\partial}{\partial \frac{dv_z}{d(ar_{\text{com}})} \Big|_{F_0, \rho_0}} \right]^2 \bar{n}_{\text{Ly}\alpha}. \end{aligned} \quad (26)$$

The number density of LAE galaxies above a flux limit can then be written as

$$n_{\text{Ly}\alpha}(> F_0) = \bar{n}_{\text{Ly}\alpha}^{(0)} [1 + \delta_g(\mathbf{x})] \left[ 1 + \bar{n}_{\text{Ly}\alpha}^{(1)} + \bar{n}_{\text{Ly}\alpha}^{(2)} \right], \quad (27)$$

where we have substituted Equation 25 into Equation 4.

To proceed further, we firstly expand the expressions in Equations 6 and 26, and then recast the above derivatives as explicit constants with respect to their radiative transfer effect. Once this has been performed, we can rewrite Equations 6 and 26 as

$$\bar{n}_{\text{Ly}\alpha}^{(1)} = \delta_\Gamma(\mathbf{x})C_\Gamma + \delta_\rho(\mathbf{x})C_\rho + \delta_v(\mathbf{x})C_v \quad (28)$$

and,

$$\begin{aligned} \bar{n}_{\text{Ly}\alpha}^{(2)} = & \frac{1}{2} [C_{\Gamma\Gamma}\delta_\Gamma^2(\mathbf{x}) + C_{\rho\rho}\delta_\rho^2(\mathbf{x}) + C_{vv}\delta_v^2(\mathbf{x})] \\ & + C_{\Gamma\rho}\delta_\Gamma(\mathbf{x})\delta_\rho(\mathbf{x}) + C_{\Gamma v}\delta_\Gamma(\mathbf{x})\delta_v(\mathbf{x}) \\ & + C_{\rho v}\delta_\rho(\mathbf{x})\delta_v(\mathbf{x}). \end{aligned} \quad (29)$$

Equations 28 and 29 contain the first- and second-order Ly $\alpha$  radiative transfer coefficients. In Appendix A we derive the explicit expressions for the first-order Ly $\alpha$  radiative transfer coefficients, and use the same basic ideas to also derive the second-order coefficients.

To the second order, the fluctuations in the number density of LAE galaxies relative to the mean are given by

$$\delta_{\text{Ly}\alpha}(\mathbf{x}) = [1 + \delta_g(\mathbf{x})] \left[ 1 + \bar{n}_{\text{Ly}\alpha}^{(1)} + \bar{n}_{\text{Ly}\alpha}^{(2)} \right] - 1. \quad (30)$$

To generate the Ly $\alpha$  radiative transfer kernels that describe the modification to the galaxy power spectrum and the higher-order corrections, we expand Equation 30 up to the second order in fluctuations, and take the Fourier transform of the corresponding expression (Appendix B). In the resulting expression, the fluctuations of the local density,  $\delta_\rho(\mathbf{x})$ , are given by Equation 20. The fluctuations in the line-of-sight peculiar velocity field in Fourier space can be expressed as  $\delta_v(\mathbf{k}) = -f\mu^2\eta(\mathbf{k})$ , where  $\eta(\mathbf{k})$  is the fluctuation in the velocity field given by Equation 21. The expression due to fluctuations in the UV background can be somewhat more complicated and is outlined in Appendix B.

In Appendix B we also derive the redshift-space expressions for the Ly $\alpha$  radiative transfer effects. Finally, in analogy with Equations 20 and 21, we write the fluctuations in the number density of LAE galaxies in real space as

$$\begin{aligned} \delta_{\text{Ly}\alpha}(\mathbf{k}, z) = & \sum_{n=1}^{\infty} D^n(z) \int \frac{d^3\mathbf{q}_1}{(2\pi)^3} \int \frac{d^3\mathbf{q}_{n-1}}{(2\pi)^3} \\ & \times \int d^3\mathbf{q}_n \delta^D(\mathbf{k} - \sum_{i=1}^n \mathbf{q}_i) Z_n^{(s)}(\mathbf{q}_1, \mathbf{q}_2, \dots, \mathbf{q}_n) \\ & \times \delta_1(\mathbf{q}_1)\delta_1(\mathbf{q}_2)\dots\delta_1(\mathbf{q}_n), \end{aligned} \quad (31)$$

and those in redshift-space as

$$\begin{aligned} \delta_{\text{Ly}\alpha,s}(\mathbf{k}, z) = & \sum_{n=1}^{\infty} D^n(z) \int \frac{d^3\mathbf{q}_1}{(2\pi)^3} \int \frac{d^3\mathbf{q}_{n-1}}{(2\pi)^3} \\ & \times \int d^3\mathbf{q}_n \delta^D(\mathbf{k} - \sum_{i=1}^n \mathbf{q}_i) K_n^{(s)}(\mathbf{q}_1, \mathbf{q}_2, \dots, \mathbf{q}_n) \\ & \times \delta_1(\mathbf{q}_1)\delta_1(\mathbf{q}_2)\dots\delta_1(\mathbf{q}_n), \end{aligned} \quad (32)$$

where the Ly $\alpha$  radiative transfer kernels,  $Z_n^{(s)}$  and  $K_n^{(s)}$ , are given in Appendix B.

### 4.4 LAE bispectrum and reduced bispectrum

The second-order terms in Equation 32 yield a non-vanishing bispectrum of the fluctuations in the number density of LAE galaxies in redshift space:

$$\begin{aligned} B_{\text{Ly}\alpha,s}(\mathbf{k}_1, \mathbf{k}_2, \mathbf{k}_3) = & 2 \left[ K_1^{(s)}(\mathbf{k}_1)K_1^{(s)}(\mathbf{k}_2)K_2^{(s)}(\mathbf{k}_1, \mathbf{k}_2) \right. \\ & \left. \times P_L(k_1)P_L(k_2) + (2 \text{ cyc.}) \right], \end{aligned} \quad (33)$$



where  $K_1^{(s)}(\mathbf{k})$  and  $K_2^{(s)}(\mathbf{k}_1, \mathbf{k}_2)$  are found in Appendix B.

The bispectrum in redshift space depends on six variables: three wavenumbers,  $k_1, k_2$ , and  $k_3$ , giving the sides of a triangle; and the cosines of the angles that these three vectors make with the line-of-sight direction,  $\mu_1, \mu_2$ , and  $\mu_3$ . However, due to the triangular condition, these six variables are not all independent. Instead, the bispectrum can be written as a function of five independent variables (Scoccimarro et al. 1999; Smith et al. 2008): three parameters ( $k_1, k_2$ , and the angle between them,  $\cos(\theta_{12})$ ) define the shape of the triangle; and the remaining two parameters ( $\mu_1$  and  $\phi$ ) define the orientation of the triangles with respect to the line-of-sight.

By convention, we align the first wavevector,  $k_1$ , to the line-of-sight direction,  $\hat{\mathbf{z}}$ , about which the triangle can be rotated through the azimuthal direction ( $\hat{\phi}$ ). The cosines of the angles that  $k_2$  and  $k_3$  make with the line-of-sight direction are given by

$$\mu_2 = \mu_1 \cos(\theta_{12}) - \sqrt{1 - \mu_1^2 \sin^2(\theta_{12})} \cos(\phi) \quad (34)$$

$$\mu_3 = -\frac{k_1}{k_3} \mu_1 - \frac{k_2}{k_3} \mu_2. \quad (35)$$

Here the last equality comes from the triangular condition,  $\mathbf{k}_1 + \mathbf{k}_2 + \mathbf{k}_3 = \mathbf{0}$ .

The ‘reduced’ bispectrum is given by the ratio of the bispectrum to the products of the power spectra:

$$Q_{\text{Ly}\alpha, s}(\mathbf{k}_1, \mathbf{k}_2, \mathbf{k}_3) \equiv \frac{B_{\text{Ly}\alpha, s}(\mathbf{k}_1, \mathbf{k}_2, \mathbf{k}_3)}{P_{\text{Ly}\alpha, s}(\mathbf{k}_1)P_{\text{Ly}\alpha, s}(\mathbf{k}_2) + 2 \text{cyc.}}. \quad (36)$$

This quantity is insensitive to the overall amplitude of the power spectrum, as the second-order expression for the bispectrum given in Equation 33 is proportional to the products of the power spectra. This properly removes the degeneracy between the galaxy bias parameters and the amplitude of the matter power spectrum.

#### 4.5 Fisher matrix

Before generating the expected cosmological constraints using the Fisher matrix, let us first summarize the model parameters characterizing the higher-order (non-linear) terms.

It is important to note that, unlike the previous work which simply multiplies the real-space bispectrum by the linear redshift distortion factors (Scoccimarro et al. 1999; Sefusatti et al. 2006; Sefusatti & Komatsu 2007), we include the *full* wavenumber dependence of the redshift-space distortion up to the second order. By including the full second-order redshift-space distortion, we gain additional information which helps to further break the degeneracies between the cosmological information and the radiative transfer effects, especially those associated with the velocity gradient.

The second-order redshift-space Ly $\alpha$  kernel, after removing the scale dependence of the ionizing background effect, is given by (see Appendix B)

$$K_2^{(s)}(\mathbf{k}_1, \mathbf{k}_2) = \frac{1}{2} \tilde{b}_2 - \frac{1}{2} f(\mu_1^2 + \mu_2^2) \tilde{C} + \tilde{b}_1 F_2^{(s)}(\mathbf{k}_1, \mathbf{k}_2) + f \mu_{12}^2 (1 - C_v) G_2^{(s)}(\mathbf{k}_1, \mathbf{k}_2) + \frac{1}{2} f^2 \mu_1^2 \mu_2^2 C_{vv}$$

$$+ \frac{1}{2} (k_{12} \mu_{12} f) \left\{ \frac{k_{1z}}{k_1^2} [\tilde{b}_1 - f \mu_2^2 C_v] + \frac{k_{2z}}{k_2^2} [\tilde{b}_1 - f \mu_1^2 C_v] \right\} + \frac{1}{2} (k_{12} \mu_{12} f)^2 \left[ \frac{k_{1z} k_{2z}}{k_1^2 k_2^2} \right] = \frac{1}{2} \tilde{b}_2 - \frac{1}{2} f(\mu_1^2 + \mu_2^2) \tilde{C} + \tilde{b}_1 F_2^{(s)}(\mathbf{k}_1, \mathbf{k}_2) + f \mu_{12}^2 (1 - C_v) G_2^{(s)}(\mathbf{k}_1, \mathbf{k}_2) + \frac{1}{2} f^2 \mu_1^2 \mu_2^2 C_{vv} + \frac{1}{2} \tilde{b}_1 (k_{12} \mu_{12} f) \left[ \frac{k_{1z}}{k_1^2} + \frac{k_{2z}}{k_2^2} \right] + \frac{1}{2} (k_{12} \mu_{12} f)^2 (1 - C_v) \left[ \frac{k_{1z} k_{2z}}{k_1^2 k_2^2} \right], \quad (37)$$

where we define

$$\tilde{b}_2 \equiv b_1^2 (C_{\Gamma\Gamma} + 2C_{\Gamma}) + C_{\rho\rho} + b_2(1 + C_{\Gamma}) + 2b_1(C_{\Gamma\rho} + C_{\rho}), \quad (38)$$

$$\tilde{C} \equiv b_1 C_v + C_{\rho v} + b_1 C_{\Gamma v}, \quad (39)$$

$$k_{ij} \equiv |\mathbf{k}_i + \mathbf{k}_j|, \quad (40)$$

$$\mu_{ij} \equiv \frac{(\mathbf{k}_i + \mathbf{k}_j) \cdot \hat{\mathbf{z}}}{|\mathbf{k}_i + \mathbf{k}_j|}, \quad (41)$$

$$k_{iz} \equiv \mathbf{k}_i \cdot \hat{\mathbf{z}}. \quad (42)$$

Here,  $\tilde{b}_2$  is the effective non-linear galaxy bias modified by various first- and second-order radiative transfer effects, and  $\tilde{b}_1$  is defined in Equation 14.

In our model, we choose to keep the second-order effect due to the peculiar velocity gradient ( $C_{vv}$ ) separate, as this has the potential to be degenerate with the growth rate of structure,  $f$ . Additionally,  $\tilde{C}$ , which contains the linear-order effects with respect to the peculiar velocity gradient, can also become degenerate with  $f$ . We note that setting the Ly $\alpha$  radiative transfer effects to zero reduces Equation 37 to the typical second-order redshift-space galaxy kernel, as required.

To generate the expected constraints on the cosmological parameters, we calculate the Fisher matrix for both the bispectrum and the reduced bispectrum. The Fisher matrix for the bispectrum is

$$F_{ij} = \sum_{k_1, k_2, k_3 \leq k_{max}} \frac{1}{\sigma_B^2} \frac{\partial B_g(k, \mu)}{\partial \theta_i} \frac{\partial B_g(k, \mu)}{\partial \theta_j}, \quad (43)$$

and for the reduced bispectrum is

$$F_{ij} = \sum_{k_1, k_2, k_3 \leq k_{max}} \frac{1}{\sigma_Q^2} \frac{\partial Q_g(k, \mu)}{\partial \theta_i} \frac{\partial Q_g(k, \mu)}{\partial \theta_j}, \quad (44)$$

where the Fisher matrices are summed over all possible triangular configurations.

The variances for the bispectrum and the reduced bispectrum are given, respectively, by

$$\sigma_B^2 = \frac{s_B V_{survey}}{N_t} P_{tot}(k_1) P_{tot}(k_2) P_{tot}(k_3) \quad (45)$$

and

$$\sigma_Q^2 = \frac{s_B V_{survey}}{N_t} \frac{P_{tot}(k_1) P_{tot}(k_2) P_{tot}(k_3)}{[P_{\text{Ly}\alpha, s}(k_1) P_{\text{Ly}\alpha, s}(k_2) + 2 \text{cyc.}]^2}. \quad (46)$$

Here  $s_B$  is the symmetric factor describing symmetry of the side lengths of a given bispectrum triangle ( $s_B =$

6, 2, 1 for equilateral, isosceles, and general triangles, respectively) and  $P_{tot}(k)$  is the sum of the power spectrum component and the Poisson shot noise:

$$P_{tot}(k) = P_{Ly\alpha,s}(k) + \frac{1}{n_g}, \quad (47)$$

where  $n_g$  is the number density of LAE galaxies. The quantity  $N_t$  is the total number of available triangles:

$$N_t = \frac{V_B}{k_F^3}, \quad (48)$$

where  $k_F$  is the fundamental frequency and

$$V_B = 2\pi d\mu d\phi k_1 k_2 k_3 (\Delta k)^3 \times \begin{cases} 1 & \text{if } k_i \neq k_j + k_k, \\ \frac{1}{2} & \text{if } k_i = k_j + k_k. \end{cases} \quad (49)$$

This states that, for ‘collapsed’ (or ‘co-linear’) triangles defined by  $k_i = k_j + k_k$ , the bispectrum volume is reduced by a factor of two. (For the derivation of  $V_B$ , see Appendix C). In the simplest spherically averaged scenario this reduces to

$$V_B = 32\pi^2 k_1 k_2 k_3 (\Delta k)^3 \times \begin{cases} 1 & \text{if } k_i \neq k_j + k_k, \\ \frac{1}{2} & \text{if } k_i = k_j + k_k. \end{cases} \quad (50)$$

## 5 CONSTRAINTS FROM THE REDUCED BISPECTRUM ALONE

In Section 3, we show that the growth rate of structure,  $f$  (or  $\tilde{\beta}$ ), is completely degenerate with the Ly $\alpha$  radiative transfer effect due to the velocity gradient,  $C_v$ , as long as we rely only on the power spectrum.

However, the bispectrum provides additional constraining power that can be used to break the degeneracy between the growth rate of structure,  $f$ , the linear galaxy bias,  $\tilde{b}_1$ , and  $C_v$ . This is because, unlike the power spectrum which just tells us the amplitude of the fluctuations at a given scale, the bispectrum tells us also *how* the structure forms. For example, one needs information in the bispectrum in order to reproduce the ‘cosmic web,’ the filamentary structures in the universe. The power spectrum cannot distinguish between the distribution with random phases and that with the filamentary structures, as it is sensitive only to the amplitude of the fluctuations. As a result, the bispectrum can distinguish between the structures caused by gravitational and non-gravitational effects.

In this section we firstly generate the expected cosmological constraints from the reduced bispectrum. As mentioned previously, the reduced bispectrum is insensitive to the amplitude of the matter power spectrum. We again consider the same two models; a fiducial model where we set the radiative transfer coefficients to be zero but marginalize over them, and a model where we use explicit values for the Ly $\alpha$  radiative transfer effects in our redshift-space expressions.

Since the recovery of the growth rate of structure  $f$  is most affected by the radiative transfer effects, we investigate the two-dimensional joint likelihood distributions for  $f$  with each of the other model parameters (marginalized over all the remaining model parameters). For the remainder of this work, we set the non-linear galaxy bias to be  $b_2 = 1.5$ .

### 5.1 Fiducial LAE reduced bispectrum

We first consider our fiducial model where we set all Ly $\alpha$  radiative transfer coefficients to zero, but marginalize over the Ly $\alpha$  effects. With the addition of the bispectrum, the number of parameters in our model has increased to eight. These include three cosmological parameters:  $f$ ,  $\ln(D_A)$ , and  $\ln(H)$ ; three radiative transfer parameters:  $C_v$ ,  $C_{vv}$ , and  $\tilde{C}$ ; and the linear and non-linear galaxy biases:  $\tilde{b}_1$  and  $\tilde{b}_2$ .

We find that the constraints generated from the reduced bispectrum contain no strong degeneracies between  $f$  and the radiative transfer parameters (see Figure 3). The reduced bispectrum does however exhibit some degeneracies between  $f$ , and the galaxy bias parameters,  $\tilde{b}_1$  and  $\tilde{b}_2$ .

To understand this result, let us write the reduced bispectrum given in Equation 36 as

$$\begin{aligned} & Q_{Ly\alpha,s}(\mathbf{k}_1, \mathbf{k}_2, \mathbf{k}_3) \\ &= \frac{2\hat{K}_1^{(s)}(\mathbf{k}_1)\hat{K}_1^{(s)}(\mathbf{k}_2)\hat{K}_2^{(s)}(\mathbf{k}_1, \mathbf{k}_2)P_L(k_1)P_L(k_2) + 2\text{cyc.}}{[\hat{K}_1^{(s)}(\mathbf{k}_1)]^2[\hat{K}_1^{(s)}(\mathbf{k}_2)]^2P_L(k_1)P_L(k_2) + 2\text{cyc.}}, \end{aligned} \quad (51)$$

where

$$\begin{aligned} \hat{K}_1^{(s)}(\mathbf{k}) &\equiv \frac{1}{\tilde{b}_1} K_1^{(s)}(\mathbf{k}) = 1 + \tilde{\beta}\mu^2(1 - C_v), \quad (52) \\ \hat{K}_2^{(s)}(\mathbf{k}_1, \mathbf{k}_2) &\equiv \frac{1}{\tilde{b}_2^2} K_2^{(s)}(\mathbf{k}_1, \mathbf{k}_2) \\ &= \frac{1}{\tilde{b}_1} \left[ \frac{1}{2} \frac{\tilde{b}_2}{\tilde{b}_1} - \frac{1}{2} \tilde{\beta}(\mu_1^2 + \mu_2^2) \tilde{C} + F_2^{(s)}(\mathbf{k}_1, \mathbf{k}_2) \right. \\ &\quad \left. + \tilde{\beta}\mu_{12}^2(1 - C_v)G_2^{(s)}(\mathbf{k}_1, \mathbf{k}_2) \right] \\ &\quad + \frac{1}{2} \tilde{\beta}(k_{12}\mu_{12}) \left[ \frac{k_{1z}}{k_1^2} + \frac{k_{2z}}{k_2^2} \right] + \mathcal{O}(\mu^4). \end{aligned} \quad (53)$$

Here,  $\mathcal{O}(\mu^4)$  are the terms that contain four powers of cosines (see Equation 37 for the full expression of  $K_2^{(s)}$ ). These terms contribute less, as their contributions are important only near the line-of-sight direction, for which the number of available modes is limited.

Equations 51, 52, and 53 show that the reduced bispectrum determines the following parameter combinations:

- $\tilde{b}_1$  from the overall amplitude of the first four terms in  $\hat{K}_2^{(s)}$ ,
- $\tilde{b}_2/\tilde{b}_1$  from a constant,  $k$ -independent term in  $\hat{K}_2^{(s)}$ ,
- $\tilde{\beta}(1 - C_v)$  from  $\hat{K}_1^{(s)}$  and the term proportional to  $G_2^{(s)}$  in  $\hat{K}_2^{(s)}$ ,
- $\tilde{\beta}\tilde{C}$  from the second term in  $\hat{K}_2^{(s)}$ , and
- $\tilde{\beta}$  from the last term before  $\mathcal{O}(\mu^4)$  in  $\hat{K}_2^{(s)}$ .

Recalling  $\tilde{\beta} = f/\tilde{b}_1$ , there are five unknown variables ( $\tilde{b}_1$ ,  $\tilde{b}_2$ ,  $f$ ,  $\tilde{C}_v$ , and  $\tilde{C}$ ), and the reduced bispectrum yields five combinations of these variables.

From the Fisher matrix calculations, we find that the reduced bispectrum primarily yields  $\tilde{b}_2/\tilde{b}_1$  and  $\tilde{\beta}$ . The information on  $\tilde{b}_1$  coming from the first four terms in  $\hat{K}_2^{(s)}$  breaks a complete degeneracy between  $\tilde{b}_2$  and  $\tilde{b}_1$  and  $f$ , but correlations between these parameters still remain. One can see this in the first two panels in Figure 3. On

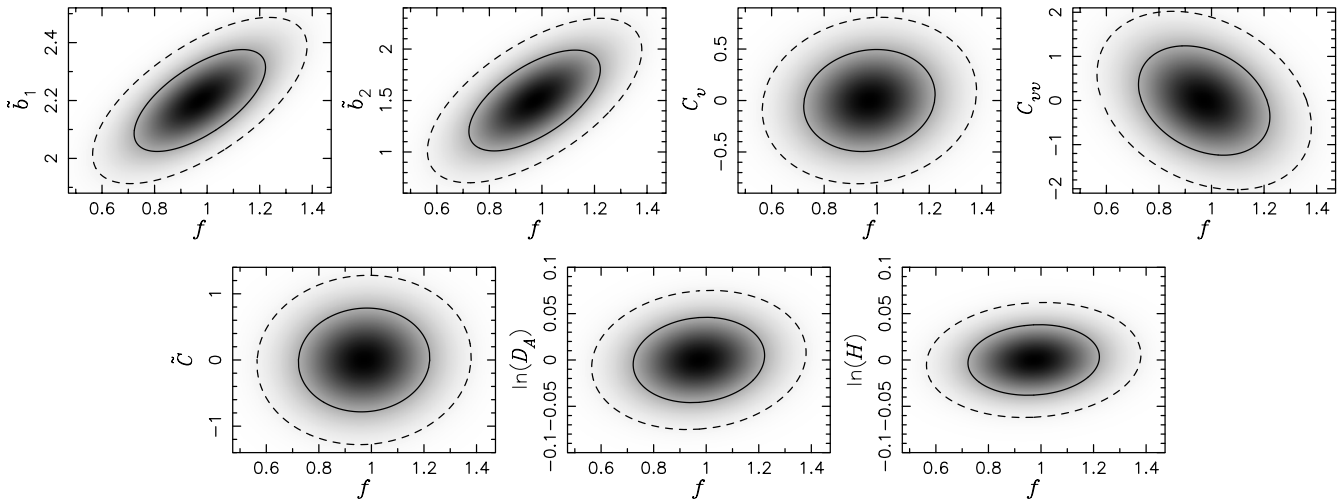


**Figure 3.** Two-dimensional joint marginalized likelihood distributions computed from the fiducial LAE galaxy *reduced* bispectrum alone (no Ly $\alpha$  radiative transfer effects, but including marginalization over  $C_v$ ,  $C_{vv}$ , and  $\tilde{C}$ ). We show the correlations between the growth rate of structure,  $f$ , and various parameters including (clockwise from top left): the linear bias,  $\tilde{b}_1$ , non-linear bias,  $\tilde{b}_2$ , linear peculiar velocity Ly $\alpha$  effect,  $C_v$ , non-linear peculiar velocity Ly $\alpha$  effect,  $C_{vv}$ , the non-linear combination of other radiative transfer effect,  $\tilde{C}$ , angular diameter distance,  $\ln(D_A)$ , and the Hubble rate  $\ln(H)$ . The solid and dashed curves show the 1- and 2- $\sigma$  joint marginalized constraints, respectively.

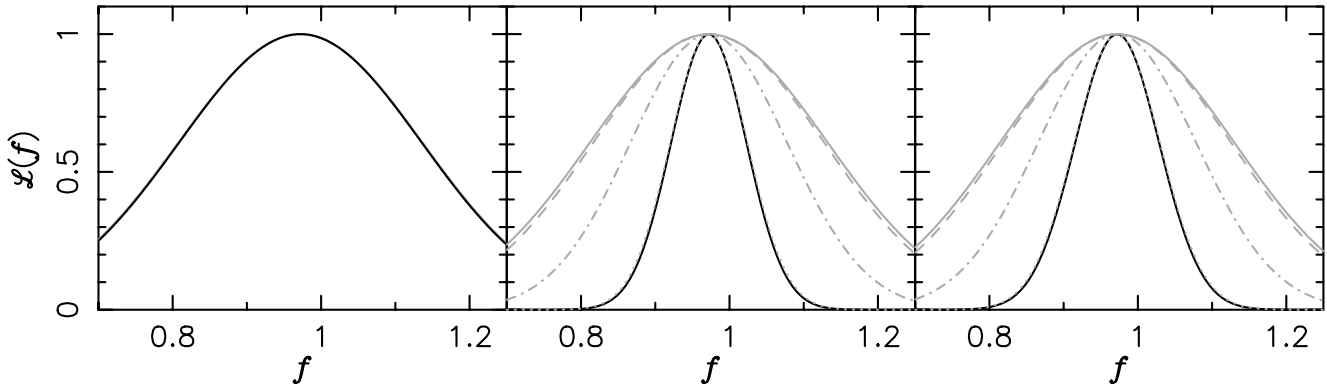


**Figure 4.** One-dimensional marginalized likelihood distributions for the growth rate of structure,  $f$ , for the fiducial case (no Ly $\alpha$  radiative effects added, but including marginalization over  $C_v$ ,  $C_{vv}$  and  $\tilde{C}$ ) generated from: (*left*) the LAE galaxy reduced bispectrum only, (*centre*) the LAE galaxy power spectrum combined with the LAE galaxy bispectrum, and (*right*) the LAE galaxy power spectrum combined with the LAE galaxy reduced bispectrum. The various curves denote different priors added to  $C_v$ ; *black solid*: Perfect knowledge of  $C_v$ , *grey dotted*:  $\sigma_{C_v} = 0.01$ , *grey dot-dashed*:  $\sigma_{C_v} = 0.1$ , *grey dashed*:  $\sigma_{C_v} = 0.5$ , and *grey solid*: no priors added.

the other hand, we do not find much correlation between  $f$  and the radiative transfer parameters,  $\tilde{C}$ ,  $\tilde{C}_v$ , and  $\tilde{C}_{vv}$  (see the third to fifth panels of Figure 3).

While the reduced bispectrum does break the degeneracy between  $f$  and  $C_v$  seen in our power spectrum analysis, it cannot provide a strong constraint on  $f$ . In the fourth column of Table 4 we provide the 1- $\sigma$  constraints generated from the one-dimensional likelihood distribution for  $f$ . In the fiducial case with no additional priors, we find the 1- $\sigma$  constraint on the growth rate of structure,  $f$ , to be 0.16 (17 per cent). It is important to note that, while the constraints are relatively weak, they are on  $f$  as opposed to  $\tilde{\beta}$ . Also,  $\tilde{\beta}$  and  $C_v$  are totally degenerate in the LAE power spectrum, and thus the error bar on  $\tilde{\beta}$  is infinite unless we put a prior on  $C_v$ . Therefore, the reduced bispectrum provides a massive improvement on

the constraint on  $f$ : the error bar shrinks from infinity to 17 per cent.

In the left panel of Figure 4, we show the one-dimensional likelihood distributions for the growth rate of structure,  $f$ , for various priors on  $C_v$ . The addition of priors to  $C_v$  does not improve the constraints on  $f$  from the reduced bispectrum alone, as the reduced bispectrum contains no degeneracy between  $f$  and  $C_v$ .

In the fourth column of Table 4 we also provide the 1- $\sigma$  constraints from the one dimensional likelihoods for  $\ln(D_A)$  and  $\ln(H)$  given various priors on  $C_v$ . We find that (independent of priors on  $C_v$ ) the fiducial LAE galaxy reduced bispectrum can recover the angular diameter distance scale at 3 per cent and the Hubble rate at 2.5 per cent. This should be contrasted with the 1.1 per cent and 1.3 per cent errors on  $D_A$  and  $H$  expected from the fiducial LAE galaxy power spectrum. Clearly the reduced

Priors on $C_v$	Parameter	Model	R BS	PS + BS	PS + R BS
			1- $\sigma$ (per cent)	1- $\sigma$ (per cent)	1- $\sigma$ (per cent)
No Priors	$f$	Fiducial	0.1645 (16.92)	0.1602 (16.48)	0.1579 (16.24)
Perfect knowledge	$f$	Fiducial	0.1635 (16.82)	0.0507 (5.21)	0.0565 (5.81)
0.01	$f$	Fiducial	0.1635 (16.82)	0.0520 (5.35)	0.0576 (5.93)
0.1	$f$	Fiducial	0.1636 (16.83)	0.1055 (10.85)	0.1063 (10.93)
0.5	$f$	Fiducial	0.1642 (16.89)	0.1555 (16.00)	0.1535 (15.79)
No Priors	$\ln(D_A)$	Fiducial	0.0303 (3.03)	0.0076 (0.76)	0.0103 (1.03)
0.01	$\ln(D_A)$	Fiducial	0.0301 (3.01)	0.0075 (0.75)	0.0101 (1.01)
0.1	$\ln(D_A)$	Fiducial	0.0302 (3.02)	0.0075 (0.75)	0.0102 (1.02)
No Priors	$\ln(H)$	Fiducial	0.0251 (2.51)	0.0084 (0.84)	0.0115 (1.15)
0.01	$\ln(H)$	Fiducial	0.0249 (2.49)	0.0083 (0.83)	0.0112 (1.12)
0.1	$\ln(H)$	Fiducial	0.0249 (2.49)	0.0083 (0.83)	0.0113 (1.13)

**Table 4.** We show the 1- $\sigma$  constraints expected from the reduced bispectrum (R BS), the power spectrum combined with the bispectrum (PS + BS), and the power spectrum combined with the reduced bispectrum (PS + R BS). No Ly $\alpha$  radiative transfer effects are included, but the likelihood is marginalized over  $C_v$ ,  $C_{vv}$ , and  $\tilde{C}$ . The first five rows show the 1- $\sigma$  constraints on  $f$  for various priors on  $C_v$ , after marginalizing over  $\tilde{b}_1$ ,  $\tilde{b}_2$ ,  $\tilde{C}$ ,  $C_v$ ,  $C_{vv}$ ,  $\ln(D_A)$ ,  $\ln(H)$ , and the amplitude  $[\ln(A)]$ . The last six rows show the 1- $\sigma$  constraints on the distance parameters,  $\ln(D_A)$  and  $\ln(H)$ , marginalized over the remaining model parameters.

Priors on $C_v$	Parameter	Model	R BS	PS + BS	PS + R BS
			1- $\sigma$ (per cent)	1- $\sigma$ (per cent)	1- $\sigma$ (per cent)
No Priors	$f$	LAE effects included	0.2104 (21.64)	0.2039 (20.97)	0.2014 (20.72)
Perfect knowledge	$f$	LAE effects included	0.2089 (21.49)	0.0632 (6.50)	0.0672 (6.91)
0.01	$f$	LAE effects included	0.2089 (21.49)	0.0645 (6.64)	0.0685 (7.05)
0.1	$f$	LAE effects included	0.2090 (21.50)	0.1262 (12.98)	0.1270 (13.06)
0.5	$f$	LAE effects included	0.2099 (21.59)	0.1965 (20.21)	0.1943 (19.99)
No Priors	$\ln(D_A)$	LAE effects included	0.0378 (3.78)	0.0099 (0.99)	0.0120 (1.20)
0.01	$\ln(D_A)$	LAE effects included	0.0376 (3.76)	0.0098 (0.98)	0.0119 (1.19)
0.1	$\ln(D_A)$	LAE effects included	0.0376 (3.76)	0.0099 (0.99)	0.0119 (1.19)
No Priors	$\ln(H)$	LAE effects included	0.0305 (3.05)	0.0107 (1.07)	0.0133 (1.33)
0.01	$\ln(H)$	LAE effects included	0.0302 (3.02)	0.0106 (1.06)	0.0131 (1.31)
0.1	$\ln(H)$	LAE effects included	0.0303 (3.03)	0.0107 (1.07)	0.0132 (1.32)

**Table 5.** Same as Table 4, but for the first-order Ly $\alpha$  radiative transfer effects given by  $C_\Gamma = 0.05$ ,  $C_\rho = -0.39$ , and  $C_v = 0.11$ .

bispectrum alone provides weaker distance constraints. This is not surprising, as the distance information is contained in the shape of the power spectrum (e.g., baryon acoustic oscillation (BAO) and Alcock-Paczynski (AP) test), which is largely divided out in the reduced bispectrum.

## 5.2 LAE reduced bispectrum

We now consider the inclusion of Ly $\alpha$  radiative transfer effects by adding the linear Ly $\alpha$  radiative transfer model parameters,  $C_\Gamma = 0.05$ ,  $C_\rho = -0.39$ , and  $C_v = 0.11$  from Wytke & Dijkstra (2011). The inclusion of these parameters modifies the effective bias parameters,  $\tilde{b}_1$  and  $\tilde{b}_2$ , and the Ly $\alpha$  radiative transfer effects associated with  $\tilde{C}$ . We still set the fiducial values of the second-order Ly $\alpha$  radiative transfer coefficients to vanish. Although we set  $C_{vv} = 0$ , we still marginalize over  $C_{vv}$  in our models.

In the fourth column of Table 5, the 1- $\sigma$  constraints on  $f$ ,  $\ln(D_A)$ , and  $\ln(H)$  are generated from the likelihood distributions for various priors on  $C_v$  as per the previous section. With the inclusion of the Ly $\alpha$  effects,

the precision with which we can constrain the growth rate of structure  $f$  has been reduced to an error of 0.21 (22 per cent) compared to 0.16 (17 per cent) for the fiducial model. Once again, this is due to the reduced effective linear galaxy bias, which reduces the signal-to-noise ratio of the LAE power spectrum relative to the shot noise.

## 6 COSMOLOGICAL CONSTRAINTS FROM COMBINING THE POWER SPECTRUM AND BISPECTRUM

We next discuss the improvements on the cosmological constraints available when we combine the LAE power spectrum with either the LAE reduced bispectrum or the bispectrum. When combining the reduced bispectrum (and the bispectrum) to the information from the power spectrum, we assume that there is no covariance between the power spectrum and the reduced bispectrum (or the bispectrum), which is incorrect. Therefore, the numerical values of the 1- $\sigma$  constraints on various parameters reported here should be considered as lower bounds.

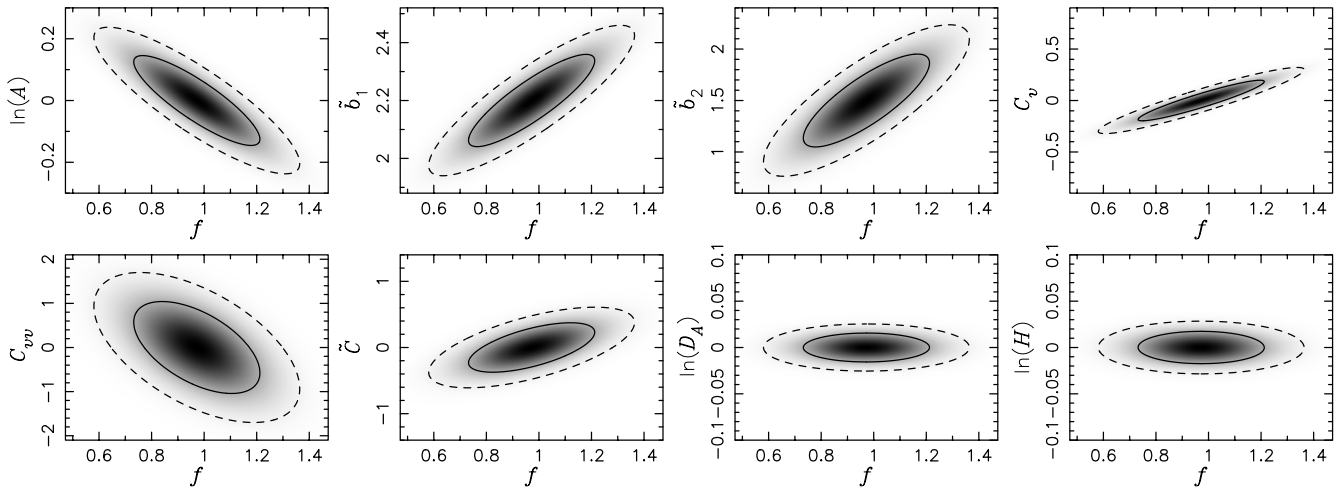


**Figure 5.** Two-dimensional joint marginalized likelihood distributions computed from the fiducial LAE galaxy power spectrum combined with the fiducial LAE galaxy *reduced* bispectrum (no Ly $\alpha$  radiative transfer effects added, but including marginalization over  $C_v$ ,  $C_{vv}$ , and  $\tilde{C}$ ). We show the correlations between the growth rate of structure,  $f$ , and various parameters including (clockwise from top left): the amplitude,  $\ln(A)$ , linear bias,  $\tilde{b}_1$ , non-linear bias,  $\tilde{b}_2$ , linear peculiar velocity Ly $\alpha$  effect,  $C_v$ , non-linear peculiar velocity Ly $\alpha$  effect,  $C_{vv}$ , the non-linear combination of other radiative transfer effect,  $\tilde{C}$ , angular diameter distance,  $\ln(D_A)$ , and the Hubble rate,  $\ln(H)$ . The solid and dashed curves show the 1- and 2- $\sigma$  joint marginalized constraints, respectively.

### 6.1 Fiducial LAE model for power spectrum and bispectrum

We first consider our fiducial model in which all Ly $\alpha$  radiative transfer coefficients are set to zero. The number of parameters in this model is nine. While the LAE galaxy reduced bispectrum is insensitive to the amplitude of the matter power spectrum, we must marginalize over the amplitude information in the LAE galaxy power spectrum. The parameters include four cosmological parameters: the amplitude [ $\ln(A)$ ],  $f$ ,  $\ln(D_A)$ , and  $\ln(H)$ ; three radiative transfer parameters:  $C_v$ ,  $C_{vv}$ , and  $\tilde{C}$ ; and the linear and non-linear galaxy biases:  $\tilde{b}_1$  and  $\tilde{b}_2$ .

#### 6.1.1 Combined power spectrum and reduced bispectrum

Figure 5 shows the expected constraints from a joint analysis of the reduced bispectrum and the power spectrum on various pairs of parameters involving  $f$ . Comparing this figure with Figure 3, we find that adding the power spectrum does not improve the constraints on  $f$  and the bias parameters very much, but improves the constraints on all the other parameters. Figure 6 shows this more clearly: adding the power spectrum information does not improve the constraint on  $f$ , but it substantially improves the constraint on  $C_v$ .

What does this imply? This implies that the uncertainty in  $f$  is now dominated by the correlation between  $f$  and the bias parameters - the correlation that we have discussed in Section 5.1. Comparing the fourth and sixth columns of Table 4 shows this quantitatively.

Comparing the fourth and sixth columns of Table 4 also shows that adding the power spectrum does improve the constraints on  $D_A$  and  $H$  substantially, as the power spectrum contains features such as BAO and AP test, whereas such information is largely cancelled out in the reduced bispectrum.

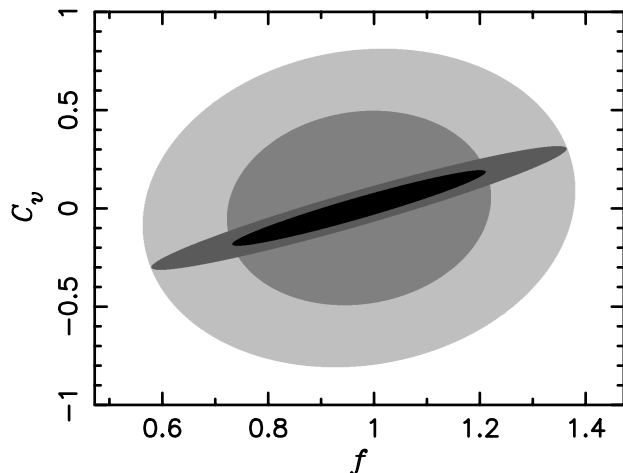


**Figure 6.** Comparison of the joint two-dimensional constraints on  $f$  and  $C_v$ . Outer two ellipses correspond to the 1- and 2- $\sigma$  constraints generated from the fiducial LAE galaxy reduced bispectrum only. Two narrower ellipses correspond to the 1- and 2- $\sigma$  constraints generated from the fiducial LAE galaxy power spectrum combined with the fiducial LAE galaxy reduced bispectrum.

Nevertheless, as the reduced bispectrum still has some sensitivity to these features (i.e., cancellation is not exact), the constraints on  $D_A$  and  $H$  from the power spectrum and the reduced bispectrum are slightly better than those from the power spectrum alone. Comparing the third column of Table 2 and the sixth columns of Table 4, we find that the expected constraints improve from 1.1 to 1.0 per cent for  $D_A$  and 1.3 to 1.2 per cent for  $H$ .

#### 6.1.2 Combined power spectrum and bispectrum

Next, we combine the power spectrum with the bispectrum (rather than the reduced bispectrum). As far as  $f$

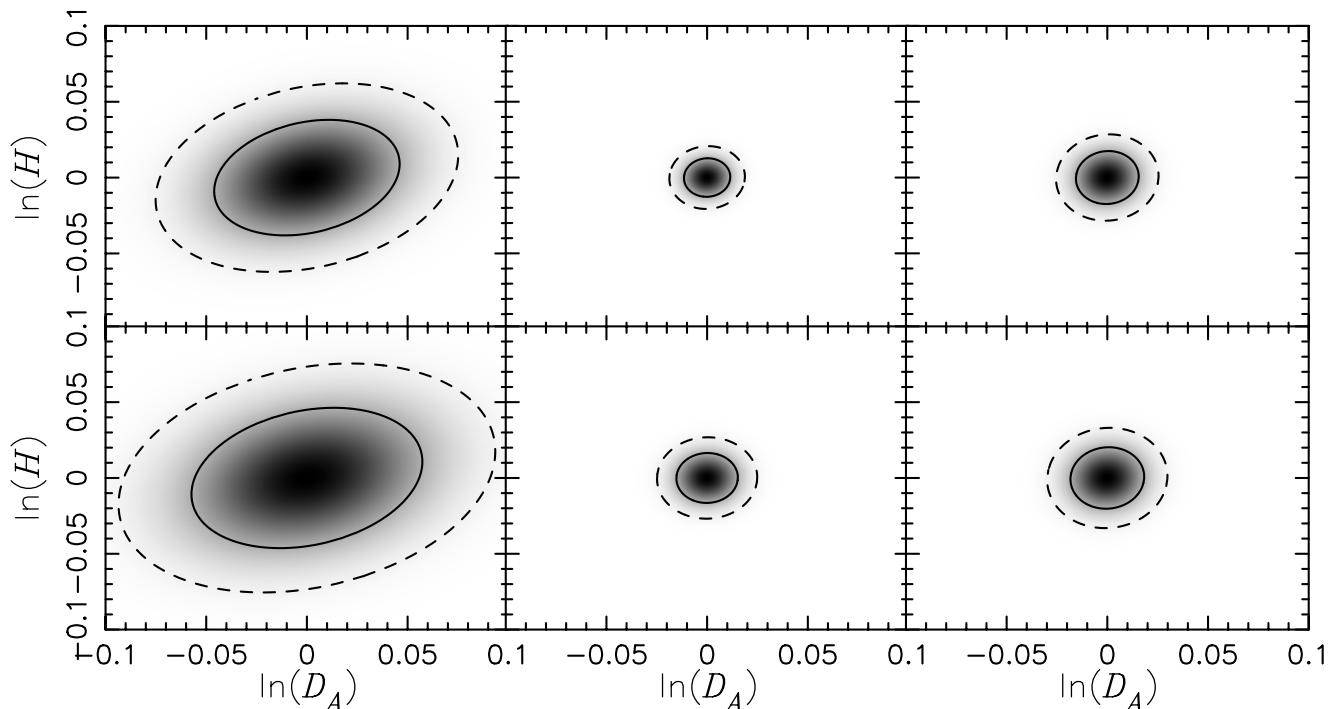


**Figure 7.** Two-dimensional joint marginalized likelihood distributions for the angular diameter distance,  $D_A$ , and the Hubble rate,  $H$ . Shown also are the 1- (solid) and 2- $\sigma$  (dashed) joint likelihood contours. From left to right show the constraints generated from the LAE galaxy reduced bispectrum only, the LAE galaxy power spectrum and bispectrum combined, and the LAE galaxy power spectrum and reduced bispectrum combined. *Top panels:* Fiducial case, with no Ly $\alpha$  radiative transfer effects added to the fiducial parameters, but marginalizing over  $C_v$ ,  $C_{vv}$ , and  $\tilde{C}$ . *Bottom panels:* The inclusion of the first-order Ly $\alpha$  radiative transfer effects,  $C_v = 0.11$ ,  $C_\Gamma = 0.05$ , and  $C_\rho = -0.39$ , and marginalizing over  $C_v$ ,  $C_{vv}$ , and  $\tilde{C}$ .

is concerned, we have the same story: adding the power spectrum does not improve the expected error bar on  $f$  (see the fifth column of Table 4).

On the other hand, a joint analysis of the power spectrum and the bispectrum yields a significant improvement on the angular diameter distance and the Hubble rate. This is because the bispectrum also contains the BAO features and the AP test in its wavenumber dependence. However, this could be due to our ignoring a covariance between the power spectrum and the bispectrum: a correlation between them would degrade the constraints in a joint analysis. This point requires a further investigation.

## 6.2 LAE model for power spectrum combined with bispectrum

Finally, we consider the inclusion of Ly $\alpha$  radiative transfer effects on the recovery on  $f$ ,  $\ln(D_A)$ , and  $\ln(H)$ , by adding the linear Ly $\alpha$  radiative transfer parameters,  $C_\Gamma = 0.05$ ,  $C_\rho = -0.39$  and  $C_v = 0.11$  from Wyithe & Dijkstra (2011). Table 5 shows the results: the expected constraints are slightly weaker than those from the fiducial case, which is again due to a smaller effective bias,  $\tilde{b}_1$ , reducing the amplitude of the signal relative to the shot noise.

## 7 SUMMARY AND CONCLUSION

In this paper we have studied how the radiative transfer effects alter the power spectrum and bispectrum of LAE galaxies, and how we can use these properties to separate the radiative transfer effects and the cosmological effects, so that we can improve the cosmological constraints derived from them.

First, as a follow up to Wyithe & Dijkstra (2011), we show that the growth rate of structure ( $f$ ) and the parameter  $C_v$  describing the radiative transfer effects of velocity gradients are completely degenerate in the linear power spectrum. Next, by performing a perturbation theory expansion of the Ly $\alpha$  radiative transfer effects, we derive the next-to-leading order corrections to the density fields of LAE galaxies. This allows us to derive the leading-order expression for the bispectrum of LAE galaxies. We then show that the reduced bispectrum alone can determine  $f$  and  $C_v$  separately, leaving no degeneracy between them. Adding the power spectrum information to the reduced bispectrum does not improve the precision of  $f$  further, as the precision of  $f$  is now limited by remaining correlations between  $f$  and the galaxy bias parameters,  $b_1$  and  $b_2$ .

We find that HETDEX-like surveys of LAE galaxies can determine  $f$  to about 20 per cent accuracy, if we do not assume any prior information on  $C_v$ . Including the prior on  $C_v$ , the uncertainty on  $f$  can be reduced down to 7 per cent. Note that this is the uncertainty on  $f$ , rather than on  $\beta = f/b_1$ .

We find that the constraints on the angular diameter

distance and the Hubble expansion rate are not directly affected by the radiative transfer parameters (with the caveat that we have assumed that the effect of the UV ionizing background fluctuation is not scale dependant). The only indirect effect is a slight reduction of the effective linear galaxy bias, which reduces the amplitude of the LAE power spectrum with respect to the shot noise, thus slightly increasing the uncertainties in the angular diameter distance and the Hubble rate. Comparison between the top and bottom panels of Figure 7 shows this graphically.

Finally, to summarize the results of this work, we provide Table 6 detailing the constraints on  $\beta$ ,  $f$ ,  $D_A$ , and  $H$  expected from HETDEX-like surveys. This table shows how powerful such surveys are in terms of measuring the distance, the expansion rate, as well as the growth rate of the structure in a high-redshift universe, and the determination of these quantities are not significantly compromised by the Ly $\alpha$  radiative transfer effect.

## ACKNOWLEDGMENTS

BG acknowledges the support of the Australian Postgraduate Award. The Centre for All-sky Astrophysics is an Australian Research Council Centre of Excellence, funded by grant CE110001020. BG would also like to acknowledge the partial travel support to the USA provided by the Astronomical Society of Australia (ASA). BG would like to thank the Texas Cosmology Center at the University of Texas at Austin for their hospitality during this work, and the Kavli Institute for the Physics and Mathematics of the Universe for their hospitality during the completion of this work. We would like to thank Donghui Jeong for helpful discussions contributing to the completion of this work as well as to the derivation provided in Appendix C. EK is supported in part by NSF grant AST-0807649 and NASA grant NNX08AL43G.

## REFERENCES

- Bernardeau F., Colombi S., Gaztañaga E., Scoccimarro R., 2002, *Physics Reports*, 367, 1
- Blake C., Brough S., Colless M., Contreras C., Couch W., Croom S., Croton D., Davis T. M., Drinkwater M. J., Forster K., Gilbank D., Gladders M., Glazebrook K., Jelliffe B., Jurek R. J., Li I.-h., Madore B., Martin D. C., Pimbblet K., Poole G. B., Pracy M., Sharp R., Wisnioski E., Woods D., Wyder T. K., Yee H. K. C., 2012, *Monthly Notices of the Royal Astronomical Society*, 425, 405
- Blake C., Brough S., Colless M., Contreras C., Couch W., Croom S., Davis T., Drinkwater M. J., Forster K., Gilbank D., Gladders M., Glazebrook K., Jelliffe B., Jurek R. J., Li I.-H., Madore B., Martin D. C., Pimbblet K., Poole G. B., Pracy M., Sharp R., Wisnioski E., Woods D., Wyder T. K., Yee H. K. C., 2011a, *Monthly Notices of the Royal Astronomical Society*, 415, 2876
- Blake C., Davis T., Poole G. B., Parkinson D., Brough S., Colless M., Contreras C., Couch W., Croom S., Drinkwater M. J., Forster K., Gilbank D., Gladders M., Glazebrook K., Jelliffe B., Jurek R. J., Li I.-H., Madore B., Martin D. C., Pimbblet K., Pracy M., Sharp R., Wisnioski E., Woods D., Wyder T. K., Yee H. K. C., 2011b, *Monthly Notices of the Royal Astronomical Society*, 415, 2892
- Blake C., Kazin E. A., Beutler F., Davis T. M., Parkinson D., Brough S., Colless M., Contreras C., Couch W., Croom S., Croton D., Drinkwater M. J., Forster K., Gilbank D., Gladders M., Glazebrook K., Jelliffe B., Jurek R. J., Li I.-H., Madore B., Martin D. C., Pimbblet K., Poole G. B., Pracy M., Sharp R., Wisnioski E., Woods D., Wyder T. K., Yee H. K. C., 2011c, *Monthly Notices of the Royal Astronomical Society*, 418, 1707
- Fry J. N., Gaztanaga E., 1993, *Astrophysical Journal*, 413, 447
- Gawiser E., Francke H., Lai K., Schawinski K., Gronwall C., Ciardullo R., Quadri R., Orsi A., Barrientos L. F., Blanc G. A., Fazio G., Feldmeier J. J., sheng Huang J., Infante L., Lira P., Padilla N., Taylor E. N., Treister E., Urry C. M., van Dokkum P. G., Virani S. N., 2007, *The Astrophysical Journal*, 671, 278
- Guaita L., Gawiser E., Padilla N., Francke H., Bond N. A., Gronwall C., Ciardullo R., Feldmeier J. J., Sinawa S., Blanc G. A., Virani S., 2010, *The Astrophysical Journal*, 714, 255
- Hill G. J., Gebhardt K., Komatsu E., Drory N., MacQueen P. J., Adams J., Blanc G. A., Koehler R., Rafal M., Roth M. M., Kelz A., Grupp F., Murphy J., Palunas P., Gronwall C., Ciardullo R., Bender R., Hopp U., Schneider D. P., 2008, *Panoramic Views of the Universe*, ASP Conf. Series, 399, 115
- Hill G. J., Gebhardt K., Komatsu E., MacQueen P. J., 2004, *The New Cosmology: Conference on Strings and Cosmology; The Mitchell Symposium on Observational Cosmology*, AIP Conference Proc., 743, 224
- Hui L., Gnedin N. Y., 1997, *Royal Astronomical Society*, 292, 27
- Iye M., Ota K., Kashikawa N., Furusawa H., Hashimoto T., Hattori T., Matsuda Y., Morokuma T., Ouchi M., Shimasaku K., 2006, *Nature*, 443, 186
- Jain B., Bertschinger E., 1994, *The Astrophysical Journal*, 431, 495
- Jeong D., Komatsu E., 2006, *The Astrophysical Journal*, 651, 619
- Kaiser N., 1984, *Astrophysical Journal*, 284, L9
- , 1987, *Royal Astronomical Society*, 227, 1
- Kashikawa N., Shimasaku K., Malkan M. A., Doi M., Matsuda Y., Ouchi M., Taniguchi Y., Ly C., Nagao T., Iye M., Motohara K., Murayama T., Murozono K., Nariai K., Ohta K., Okamura S., Sasaki T., Shioya Y., Umemura M., 2006, *The Astrophysical Journal*, 648, 7
- Komatsu E., Smith K. M., Dunkley J., Bennett C. L., Gold B., Hinshaw G., Jarosik N., Larson D., Nolte M. R., Page L., Spergel D. N., Halpern M., Hill R. S., Kogut A., Limon M., Meyer S. S., Odegard N., Tucker G. S., Weiland J. L., Wollack E., Wright E. L., 2011, *The Astrophysical Journal Supplement*, 192, 18
- Kovač K., Somerville R. S., Rhoads J. E., Malhotra S., Wang J., 2007, *The Astrophysical Journal*, 668, 15
- Laursen P., Sommer-Larsen J., Razoumov A. O., 2011, *The Astrophysical Journal*, 728, 52
- Lehnert M. D., Nesvadba N. P. H., Cuby J.-G., Swin-

Priors on $C_v$	Parameter	Model	PS		R BS		PS + BS		PS + R BS	
			1- $\sigma$	per cent	1- $\sigma$	per cent	1- $\sigma$	per cent	1- $\sigma$	per cent
No Priors	$\beta$	Galaxy	0.0213	4.8	-	-	-	-	-	-
No Priors	$f$	Fiducial	-	-	0.1645	16.9	0.1602	16.5	0.1579	16.2
0.01	$f$	Fiducial	0.0218 ( $\tilde{\beta}$ )	4.9	0.1635	16.8	0.0520	5.3	0.0576	5.9
0.1	$f$	Fiducial	0.0491 ( $\tilde{\beta}$ )	11.1	0.1636	16.8	0.1055	10.9	0.1063	10.9
No Priors	$f$	LAE effects	-	-	0.2104	21.6	0.2039	21.0	0.2014	20.7
0.01	$f$	LAE effects	0.0283 ( $\tilde{\beta}$ )	5.6	0.2089	21.5	0.0645	6.7	0.0685	7.1
0.1	$f$	LAE effects	0.0633 ( $\tilde{\beta}$ )	12.5	0.2090	21.5	0.1262	13.0	0.1270	13.1
No Priors	$\ln(D_A)$	Fiducial	0.0110	1.10	0.0303	3.03	0.0076	0.76	0.0103	1.03
No Priors	$\ln(D_A)$	LAE effects	0.0128	1.28	0.0378	3.78	0.0099	0.99	0.0120	1.20
No Priors	$\ln(H)$	Fiducial	0.0132	1.32	0.0251	2.51	0.0084	0.84	0.0115	1.15
No Priors	$\ln(H)$	LAE effects	0.0151	1.51	0.0305	3.05	0.0107	1.07	0.0133	1.33

**Table 6.** Summary table of the relevant 1- $\sigma$  constraints (and fractional errors) generated from the one-dimensional likelihood distributions for  $\beta$ ,  $f$ ,  $\ln(D_A)$ , and  $\ln(A)$ . Models considered are ‘Galaxy’ (no Ly $\alpha$  radiative transfer effects, and no marginalization over the radiative transfer parameters), ‘Fiducial’ (no Ly $\alpha$  radiative transfer effects, but marginalized over the radiative transfer parameters), and ‘LAE effects’ (non-zero Ly $\alpha$  radiative transfer parameters are included and marginalized over). We consider a power spectrum only model (PS), reduced bispectrum only (R BS), power spectrum combined with the bispectrum (PS + BS), and the power spectrum combined with the reduced bispectrum (PS + R BS). We explore three priors on the Ly $\alpha$  radiative parameter associated with the peculiar velocity,  $C_v$ : no prior at all, prior of 0.01, and prior of 0.1.

bank A. M., Morris S., Clément B., Evans C. J., Bremer M. N., Basa S., 2010, *Nature*, 467, 940, (c) 2010: *Nature*

Linder E. V., 2005, *Physical Review D*, 72, 43529

McDonald P., 2006, *Physical Review D*, 74, 103512

Morales M. F., Wyithe J. S. B., 2010, *Annual Review of Astronomy and Astrophysics*, 48, 127

Orsi A., Lacey C. G., Baugh C. M., Infante L., 2008, *Monthly Notices of the Royal Astronomical Society*, 391, 1589

Ouchi M., Shimasaku K., Furusawa H., Saito T., Yoshida M., Akiyama M., Ono Y., Yamada T., Ota K., Kashikawa N., Iye M., Kodama T., Okamura S., Simpson C., Yoshida M., 2010, *The Astrophysical Journal*, 723, 869

Scoccimarro R., Couchman H. M. P., Frieman J. A., 1999, *The Astrophysical Journal*, 517, 531

Sefusatti E., Crocce M., Pueblas S., Scoccimarro R., 2006, *Physical Review D*, 74, 23522

Sefusatti E., Komatsu E., 2007, *Physical Review D*, 76, 83004

Seo H.-J., Eisenstein D. J., 2003, *The Astrophysical Journal*, 598, 720

Shoji M., Jeong D., Komatsu E., 2009, *The Astrophysical Journal*, 693, 1404

Smith R. E., Sheth R. K., Scoccimarro R., 2008, *Physical Review D*, 78, 23523

Wyithe J. S. B., Dijkstra M., 2011, *Monthly Notices of the Royal Astronomical Society*, 415, 3929

Yoshikawa K., Taruya A., Jing Y. P., Suto Y., 2001, *The Astrophysical Journal*, 558, 520

Zheng Z., Cen R., Trac H., Miralda-Escudé J., 2010, *The Astrophysical Journal*, 716, 574

—, 2011, *The Astrophysical Journal*, 726, 38

## APPENDIX A: Ly $\alpha$ RADIATIVE TRANSFER COEFFICIENTS

Throughout this work, we denote the Ly $\alpha$  radiative transfer effects as constants, which encompass the derivatives of the transmission function with respect to the Ly $\alpha$  radiative transfer effect. Here we outline the derivations for the first-order Ly $\alpha$  radiative transfer coefficients, from which the second-order constants can be easily calculated. In the following derivations, each of the Ly $\alpha$  radiative transfer effects is expressed as a function of an arbitrary transmission function,  $\mathcal{T}$  (Wyithe & Dijkstra 2011).

First, let us consider the fluctuations in the ionizing background, which are taken from the expression in Equation 6,

$$\begin{aligned}
& \left. \frac{(\Gamma - \Gamma_0)}{\bar{n}_{\text{Ly}\alpha}^{(0)}} \frac{\partial \bar{n}_{\text{Ly}\alpha}}{\partial \Gamma} \right|_{F_0, \Gamma_0} \\
&= \left( \frac{\Gamma - \Gamma_0}{\bar{n}_{\text{Ly}\alpha}^{(0)} \Gamma_0} \right) \left. \frac{\partial \log(\mathcal{T})}{\partial \log(\Gamma)} \right|_{\Gamma_0, \Gamma_0} \left. \frac{\partial \bar{n}_{\text{Ly}\alpha}}{\partial \log(\mathcal{T})} \right|_{F_0, \mathcal{T}_0} \\
&\equiv \delta_\Gamma C_\Gamma,
\end{aligned} \tag{A1}$$

where we have defined  $\delta_\Gamma \equiv \left( \frac{\Gamma - \Gamma_0}{\Gamma_0} \right)$  and

$$C_\Gamma \equiv \frac{1}{\bar{n}_{\text{Ly}\alpha}^{(0)}} \left. \frac{\partial \log(\mathcal{T})}{\partial \log(\Gamma)} \right|_{\Gamma_0, \Gamma_0} \left. \frac{\partial \bar{n}_{\text{Ly}\alpha}}{\partial \log(\mathcal{T})} \right|_{F_0, \mathcal{T}_0}. \tag{A2}$$

Following the same idea, we redefine the other two terms in Equation 6 as fluctuations in the density field, and in the line-of-sight velocity field. For the density field, we find

$$\frac{1}{\bar{n}_{\text{Ly}\alpha}^{(0)}} (\rho - \rho_0) \left. \frac{\partial \bar{n}_{\text{Ly}\alpha}}{\partial \rho} \right|_{F_0, \rho_0} \equiv \delta_\rho C_\rho, \tag{A3}$$



where

$$C_\rho \equiv \frac{1}{\bar{n}_{\text{Ly}\alpha}^{(0)}} \left. \frac{\partial \log(\mathcal{T})}{\partial \log(\rho)} \right|_{\mathcal{T}_0, \rho_0} \frac{\partial \bar{n}_{\text{Ly}\alpha}}{\partial \log(\mathcal{T})} \Big|_{F_0, \mathcal{T}_0}. \quad (\text{A4})$$

However for the velocity gradient, we rewrite the derivative as

$$\begin{aligned} & \frac{1}{\bar{n}_{\text{Ly}\alpha}^{(0)}} \left( \frac{dv_z}{d(ar_{\text{com}})} - H \right) \frac{\partial \bar{n}_{\text{Ly}\alpha}}{\partial \left( \frac{dv_z}{d(ar_{\text{com}})} \right)} \Big|_{F_0, \rho_0} \\ &= \frac{1}{\bar{n}_{\text{Ly}\alpha}^{(0)}} \frac{1}{a} \left( \frac{dv_z}{d(r_{\text{com}})} - Ha \right) \frac{\partial \bar{n}_{\text{Ly}\alpha}}{\left( \frac{1}{a} \right) \partial \left( \frac{dv_z}{dr_{\text{com}}} \right)} \Big|_{F_0, \rho_0} \\ &= \frac{dv_{\text{pec}}}{d(r_{\text{com}})} \frac{\partial \bar{n}_{\text{Ly}\alpha}}{\partial \left( \frac{dv_z}{dr_{\text{com}}} \right)} \Big|_{F_0, \rho_0}, \end{aligned} \quad (\text{A5})$$

where we have expressed the total velocity as  $v = H(ar_{\text{com}}) + v_{\text{pec}}$ , yielding the velocity gradient

$$\frac{dv}{d(r_{\text{com}})} = Ha + \frac{dv_{\text{pec}}}{d(r_{\text{com}})}. \quad (\text{A6})$$

Following the case for the ionizing background, we rewrite the partial derivative as

$$\begin{aligned} & \frac{\partial \bar{n}_{\text{Ly}\alpha}}{\partial \left( \frac{dv_z}{dr_{\text{com}}} \right)} \Big|_{F_0, \rho_0} \\ &= \frac{\partial \log(\mathcal{T})}{\partial \log \left( \frac{dv_z}{dr_{\text{com}}} \right)} \Big|_{\mathcal{T}_0, \rho_0} \frac{\partial \log \left( \frac{dv_z}{dr_{\text{com}}} \right)}{\partial \left( \frac{dv_z}{dr_{\text{com}}} \right)} \Big|_0 \frac{\partial \bar{n}_{\text{Ly}\alpha}}{\partial \log(\mathcal{T})} \Big|_{F_0, \mathcal{T}_0}. \end{aligned} \quad (\text{A7})$$

Using

$$\left( \frac{dv_z}{dr_{\text{com}}} \right)_0 = Ha, \quad (\text{A8})$$

$$\frac{\partial \log \left( \frac{dv_z}{dr_{\text{com}}} \right)}{\partial \left( \frac{dv_z}{dr_{\text{com}}} \right)} \Big|_0 = \frac{1}{Ha}, \quad (\text{A9})$$

we find

$$\begin{aligned} & \frac{1}{\bar{n}_{\text{Ly}\alpha}^{(0)}} \left( \frac{dv_z}{d(ar_{\text{com}})} - H \right) \frac{\partial \bar{n}_{\text{Ly}\alpha}}{\partial \left( \frac{dv_z}{d(ar_{\text{com}})} \right)} \Big|_{F_0, \rho_0} \\ &= \frac{1}{\bar{n}_{\text{Ly}\alpha}^{(0)}} \frac{1}{Ha} \frac{dv_{\text{pec}}}{d(r_{\text{com}})} \frac{\partial \log(\mathcal{T})}{\partial \log \left( \frac{dv_z}{dr_{\text{com}}} \right)} \Big|_{\mathcal{T}_0, \rho_0} \frac{\partial \bar{n}_{\text{Ly}\alpha}}{\partial \log(\mathcal{T})} \Big|_{F_0, \mathcal{T}_0} \\ &\equiv C_v \delta_v, \end{aligned} \quad (\text{A10})$$

where  $\delta_v \equiv \frac{1}{Ha} \frac{dv_{\text{pec}}}{d(r_{\text{com}})}$ , and

$$C_v \equiv \frac{1}{\bar{n}_{\text{Ly}\alpha}^{(0)}} \frac{\partial \log(\mathcal{T})}{\partial \log \left( \frac{dv_z}{dr_{\text{com}}} \right)} \Big|_{\mathcal{T}_0, \rho_0} \frac{\partial \bar{n}_{\text{Ly}\alpha}}{\partial \log(\mathcal{T})} \Big|_{F_0, \mathcal{T}_0}. \quad (\text{A11})$$

## APPENDIX B: Ly $\alpha$ RADIATIVE TRANSFER KERNELS

Here we outline the derivation of the higher-order real- and redshift-space kernels for the fluctuations in the number density of LAEs.

### B1 Real-space Ly $\alpha$ kernels

In this subsection, we derive the symmetrized kernels,  $Z_n^{(s)}$ , which give the LAE galaxies in real space as

$$\begin{aligned} \delta_{\text{Ly}\alpha}(\mathbf{k}, z) &= \sum_{n=1}^{\infty} D^n(z) \int \frac{d^3 \mathbf{q}_1}{(2\pi)^3} \int \frac{d^3 \mathbf{q}_{n-1}}{(2\pi)^3} \\ &\quad \times \int d^3 \mathbf{q}_n \delta^D(\mathbf{k} - \sum_{i=1}^n \mathbf{q}_i) Z_n^{(s)}(\mathbf{q}_1, \mathbf{q}_2, \dots, \mathbf{q}_n) \\ &\quad \times \delta_1(\mathbf{q}_1) \delta_1(\mathbf{q}_2) \dots \delta_1(\mathbf{q}_n). \end{aligned} \quad (\text{B1})$$

Expanding out Equation 30 and keeping terms only to second order in fluctuations,

$$\delta_{\text{Ly}\alpha}(\mathbf{x}) = \delta_g(\mathbf{x}) + \bar{n}_{\text{Ly}\alpha}^{(1)} + \bar{n}_{\text{Ly}\alpha}^{(2)} + \delta_g(\mathbf{x}) \bar{n}_{\text{Ly}\alpha}^{(1)}. \quad (\text{B2})$$

Now, substituting in Equations 24, 28 and 29 into Equation B2 and expanding, again only keeping terms up to the second order in fluctuations,

$$\begin{aligned} & \delta_{\text{Ly}\alpha}(\mathbf{x}) \\ &= b_1 \delta(\mathbf{x}) + \frac{1}{2} b_2 \delta(\mathbf{x})^2 + \delta_\Gamma(\mathbf{x}) C_\Gamma + \delta_\rho(\mathbf{x}) C_\rho + \delta_v(\mathbf{x}) C_v \\ &\quad + \frac{1}{2} [C_\Gamma \delta_\Gamma^2(\mathbf{x}) + C_{\rho\rho} \delta_\rho^2(\mathbf{x}) + C_{vv} \delta_v^2(\mathbf{x})] \\ &\quad + C_{\Gamma\rho} \delta_\Gamma(\mathbf{x}) \delta_\rho(\mathbf{x}) + C_{\Gamma v} \delta_\Gamma(\mathbf{x}) \delta_v(\mathbf{x}) + C_{\rho v} \delta_\rho(\mathbf{x}) \delta_v(\mathbf{x}) \\ &\quad + b_1 \delta(\mathbf{x}) [\delta_\Gamma(\mathbf{x}) C_\Gamma + \delta_\rho(\mathbf{x}) C_\rho + \delta_v(\mathbf{x}) C_v]. \end{aligned} \quad (\text{B3})$$

To model the effect of the fluctuating ionizing background, we convolve the overdensity of sources (in this case the galaxies),  $\delta_g(\mathbf{x})$ , with a function of the form  $\propto \exp[-(\mathbf{x} - \mathbf{x}_o)/\lambda]/[(\mathbf{x} - \mathbf{x}_o)^2]$  (Morales & Wyithe 2010), where  $\lambda$  is the mean free path of the ionizing photons. Hence we find the Fourier transform of the ionizing fluctuations as

$$\delta_\Gamma(\mathbf{k}) = \delta_g(\mathbf{k}) \frac{\arctan(|\mathbf{k}|\lambda)}{|\mathbf{k}|\lambda}, \quad (\text{B4})$$

which, to the second order, yields

$$\delta_\Gamma(\mathbf{k}) = \left[ b_1 \delta(\mathbf{k}) + \frac{1}{2} b_2 \delta(\mathbf{k})^2 \right] \frac{\arctan(|\mathbf{k}|\lambda)}{|\mathbf{k}|\lambda}. \quad (\text{B5})$$

Taking the Fourier transform of Equation B3, and using Equation 20, 21, and B5 for the density field, peculiar-velocity field, and the ionizing background, respectively, and again keeping terms up to the second order only, one finally obtains

$$\begin{aligned} \delta_{\text{Ly}\alpha}(\mathbf{k}) &= [b_1 + C_\Gamma b_1 A(\mathbf{k}) + C_\rho] \delta^{(1)}(\mathbf{k}) + C_v \delta_v^{(1)}(\mathbf{k}) \\ &\quad + [b_1 + C_\Gamma b_1 A(\mathbf{q}_1, \mathbf{q}_2) + C_\rho] \delta^{(2)}(\mathbf{q}_1, \mathbf{q}_2) \\ &\quad + C_v \delta_v^{(2)}(\mathbf{q}_1, \mathbf{q}_2) + \left[ \frac{1}{2} b_2 + \frac{1}{2} C_\Gamma b_2 A(\mathbf{q}_1, \mathbf{q}_2) \right. \\ &\quad + \frac{1}{2} C_\Gamma b_1^2 A(\mathbf{q}_1) A(\mathbf{q}_2) + \frac{1}{2} C_{\rho\rho} + C_{\Gamma\rho} b_1 A(\mathbf{q}_1) \\ &\quad + b_1^2 C_\Gamma A(\mathbf{q}_1) + b_1 C_\rho] \delta^{(1)}(\mathbf{q}_1) \delta^{(1)}(\mathbf{q}_2) \\ &\quad + [C_{\Gamma v} b_1 A(\mathbf{q}_1) + C_{\rho v} + b_1 C_v] \delta^{(1)}(\mathbf{q}_1) \delta_v^{(1)}(\mathbf{q}_2) \\ &\quad + \frac{1}{2} C_{vv} \delta_v^{(1)}(\mathbf{q}_1) \delta_v^{(1)}(\mathbf{q}_2), \end{aligned} \quad (\text{B6})$$

where  $\mathbf{k} = \mathbf{q}_1 + \mathbf{q}_2$ ,  $A(\mathbf{q}_1) \equiv \frac{\arctan(|\mathbf{q}_1|\lambda)}{|\mathbf{q}_1|\lambda}$ , and  $A(\mathbf{q}_1, \mathbf{q}_2) \equiv \frac{\arctan(|\mathbf{q}_1 + \mathbf{q}_2|\lambda)}{|\mathbf{q}_1 + \mathbf{q}_2|\lambda}$ . Where also,  $\delta^{(1)}(\mathbf{k})$  is read as the  $n = 1$  term and  $\delta^{(2)}(\mathbf{q}_1, \mathbf{q}_2)$  is read as the  $n = 2$  term of

Equation 20. In the peculiar-velocity effects,  $\delta_v^{(1)}(\mathbf{k}) = -f\mu^2\eta^{(1)}(\mathbf{k})$  and  $\delta_v^{(2)}(\mathbf{q}_1, \mathbf{q}_2) = -f\mu_1^2\eta^{(2)}(\mathbf{k})$ , the terms  $\eta^{(1)}(\mathbf{k})$  and  $\eta^{(2)}(\mathbf{k})$  are the  $n = 1$  and  $n = 2$  terms of Equation 21, respectively. In the above expression,  $\mu$  is the cosine of the angle between the line-of-sight vector,  $\hat{\mathbf{z}}$ , and the wavevector,  $\mathbf{k}$ , i.e.,  $\mu \equiv \mathbf{k} \cdot \hat{\mathbf{z}}/k$ , and  $f = \frac{d \ln D(a)}{d \ln a}$  is the growth rate of structure whose derivative is a function of the scale factor,  $a$ .

After we symmetrize the above expression and collect into first- and second-order expressions, we obtain the first- and second-order real-space kernels as

$$Z_1^{(s)}(\mathbf{k}) = b_1 \left( 1 + C_\Gamma \frac{\arctan(|\mathbf{k}|\lambda)}{|\mathbf{k}|\lambda} \right) + C_\rho - f\mu^2 C_v \quad (\text{B7})$$

$$\begin{aligned} Z_2^{(s)}(\mathbf{q}_1, \mathbf{q}_2) &= \frac{1}{2} b_1^2 C_{\Gamma\Gamma} A(\mathbf{q}_1) A(\mathbf{q}_2) + \frac{1}{2} C_{\rho\rho} + b_1 C_\rho \\ &+ \frac{b_2}{2} [1 + C_\Gamma A(\mathbf{q}_1, \mathbf{q}_2)] - \frac{1}{2} f C_{\rho v} (\mu_1^2 + \mu_2^2) \\ &+ \frac{1}{2} b_1 (C_{\Gamma\rho} + b_1 C_\Gamma) [A(\mathbf{q}_1) + A(\mathbf{q}_2)] \\ &- \frac{1}{2} b_1 C_v f (\mu_1^2 + \mu_2^2) - f \mu_{12}^2 C_v G_2^{(s)}(\mathbf{q}_1, \mathbf{q}_2) \\ &+ \{b_1 [1 + C_\Gamma A(\mathbf{q}_1, \mathbf{q}_2)] + C_\rho\} F_2^{(s)}(\mathbf{q}_1, \mathbf{q}_2) \\ &- \frac{1}{2} f b_1 C_{\Gamma v} [\mu_2^2 A(\mathbf{q}_1) + \mu_1^2 A(\mathbf{q}_2)] \\ &+ \frac{1}{2} f^2 \mu_1^2 \mu_2^2 C_{vv}. \end{aligned} \quad (\text{B8})$$

## B2 Redshift-space Ly $\alpha$ kernels

In this subsection, we derive the symmetrized kernels,  $K_n^{(s)}$ , which give the LAE galaxies in redshift space as

$$\begin{aligned} \delta_{\text{Ly}\alpha, s}(\mathbf{k}, z) &= \sum_{n=1}^{\infty} D^n(z) \int \frac{d^3 \mathbf{q}_1}{(2\pi)^3} \int \frac{d^3 \mathbf{q}_{n-1}}{(2\pi)^3} \\ &\times \int d^3 \mathbf{q}_n \delta^D(\mathbf{k} - \sum_{i=1}^n \mathbf{q}_i) K_n^{(s)}(\mathbf{q}_1, \mathbf{q}_2, \dots, \mathbf{q}_n) \\ &\times \delta_1(\mathbf{q}_1) \delta_1(\mathbf{q}_2) \dots \delta_1(\mathbf{q}_n), \end{aligned} \quad (\text{B9})$$

In galaxy redshift surveys we measure positions of galaxies in redshift space as opposed to real space. To generate the redshift-space expressions for the Ly $\alpha$  kernels we perform the following coordinate transform:

$$\mathbf{s} = \mathbf{x} + (1+z) \frac{v(\mathbf{x}) \cdot \hat{\mathbf{z}}}{H(z)}, \quad (\text{B10})$$

where  $\mathbf{s}$  denotes redshift space and  $v(\mathbf{x})$  is the line-of-sight peculiar velocity. We assume the standard ‘plane-parallel approximation,’ in which the peculiar velocity vector and the line-of-sight direction are parallel (or anti-parallel), and are chosen to be along the  $\hat{\mathbf{z}}$ -direction. In other words, we ignore curvature of the sky. We can rewrite Equation B11 as

$$\mathbf{s} = \mathbf{x} + f u_z(\mathbf{x}) \hat{\mathbf{z}}, \quad (\text{B11})$$

where  $\mathbf{u}(\mathbf{x}) \equiv (1+z) \frac{v(\mathbf{x})}{fH(z)}$ . We can then relate the fluctuations in real space and redshift space using the mass conservation:

$$[1 + \delta_{\text{Ly}\alpha, s}(\mathbf{s})] d^3 \mathbf{s} = [1 + \delta_{\text{Ly}\alpha}(\mathbf{x})] d^3 \mathbf{x}. \quad (\text{B12})$$

Taking the Fourier transform of both sides, yields the exact expression relating the real and redshift space quantities:

$$\begin{aligned} \delta_{\text{Ly}\alpha, s}(\mathbf{k}) &= \delta_{\text{Ly}\alpha}(\mathbf{k}) \\ &+ \int d^3 x e^{-i\mathbf{k} \cdot \mathbf{x}} \left( e^{-ik_z f u_z} - 1 \right) [1 + \delta_{\text{Ly}\alpha}(\mathbf{x})], \end{aligned} \quad (\text{B13})$$

where  $u_z(\mathbf{k}, z) \equiv -\frac{if}{k} \eta(\mathbf{k}, z)$ , and  $\eta(\mathbf{k}, z)$  is given by Equation 21. Expanding the exponential as a power series and keeping terms up to the second order only,

$$\begin{aligned} \delta_{\text{Ly}\alpha, s}(\mathbf{k}) &= \delta_{\text{Ly}\alpha}(\mathbf{k}) - \delta_v(\mathbf{k}) - \int d^3 x e^{-i\mathbf{k} \cdot \mathbf{x}} \\ &\times \left[ ik_z f u_z(\mathbf{x}) \delta_{\text{Ly}\alpha}(\mathbf{x}) + \frac{1}{2} k_z^2 f^2 u_z^2(\mathbf{x}) \right]. \end{aligned} \quad (\text{B14})$$

Now, inserting Equations 21 and 31 into B14, and symmetrizing the arguments, we obtain the first- and the second-order redshift-space kernels as

$$\begin{aligned} K_1^{(s)}(\mathbf{k}) &= b_1 [1 + C_\Gamma A(\mathbf{k})] + C_\rho + f\mu^2(1 - C_v), \quad (\text{B15}) \\ K_2^{(s)}(\mathbf{q}_1, \mathbf{q}_2) &= Z_2^{(s)}(\mathbf{q}_1, \mathbf{q}_2) + f\mu_{12}^2 G_2^{(s)}(\mathbf{q}_1, \mathbf{q}_2) \\ &+ \frac{1}{2} (q_{12} \mu_{12} f)^2 \left[ \frac{q_{1z} q_{2z}}{q_1^2 q_2^2} \right] \\ &+ \frac{1}{2} (q_{12} \mu_{12} f) \left[ \frac{q_{1z}}{q_1^2} Z_1^{(s)}(\mathbf{q}_2) + \frac{q_{2z}}{q_2^2} Z_1^{(s)}(\mathbf{q}_1) \right], \end{aligned} \quad (\text{B16})$$

where

$$\mu_{12} \equiv (\mathbf{q}_1 + \mathbf{q}_2) \cdot \hat{\mathbf{z}}/q_{12}, \quad (\text{B17})$$

$$q_{12} \equiv |\mathbf{q}_1 + \mathbf{q}_2|, \quad (\text{B18})$$

$$q_{1z} \equiv \mathbf{q}_1 \cdot \hat{\mathbf{z}} = q_1 \mu_1. \quad (\text{B19})$$

## APPENDIX C: CALCULATION OF $V_B$

To calculate the sample variance of the bispectrum (and reduced bispectrum), we need the volume of the bispectrum estimator,  $V_B$ , used in Equation 48, which determines the number of triangular configurations sampled at each position. We begin with the definition of  $V_B$ :

$$V_B = \int_{\mathbf{k}_1} d^3 q_1 \int_{\mathbf{k}_2} d^3 q_2 \int_{\mathbf{k}_3} d^3 q_3 \delta^D(\mathbf{q}_{123}). \quad (\text{C1})$$

Rewriting  $\delta^D(\mathbf{q}_{123})$ , we find

$$V_B = \int \frac{d^3 x}{(2\pi)^3} \int_{\mathbf{k}_1} d^3 q_1 e^{i\mathbf{x} \cdot \mathbf{q}_1} \int_{\mathbf{k}_2} d^3 q_2 e^{i\mathbf{x} \cdot \mathbf{q}_2} \int_{\mathbf{k}_3} d^3 q_3 e^{i\mathbf{x} \cdot \mathbf{q}_3}.$$

Now

$$\begin{aligned} \int_{\mathbf{k}_3} d^3 q_3 e^{i\mathbf{x} \cdot \mathbf{q}_3} &\simeq 4\pi \left[ k_3 \frac{\sin(k_3 x)}{x} \Delta k + O(\Delta k^3) \right] \\ &\simeq 4\pi k_3 \frac{\sin(k_3 x)}{x} \Delta k, \end{aligned} \quad (\text{C2})$$

yielding

$$V_B = 32\pi k_1 k_2 k_3 (\Delta k)^3 \int_0^\infty \frac{\sin(k_1 x) \sin(k_2 x) \sin(k_3 x)}{x} dx. \quad (\text{C3})$$

Evaluating the integral,

$$\begin{aligned}
& \int_0^\infty \frac{\sin(k_1 x) \sin(k_2 x) \sin(k_3 x)}{x} dx \\
&= \frac{1}{2} \int_{-\infty}^\infty \left( \frac{\sin(k_1 x)}{x} \right) \sin(k_2 x) \sin(k_3 x) dx \\
&= \frac{1}{2} \int_{-\infty}^\infty \left( \frac{1}{2} k_1 \int_{-1}^1 e^{ix k_1 \mu} d\mu \right) \sin(k_2 x) \sin(k_3 x) dx \\
&= -\frac{\pi}{8} k_1 \int_{-1}^1 d\mu \int_{-\infty}^\infty \frac{dx}{2\pi} \left[ e^{ix(k_1 \mu + k_2 + k_3)} - e^{ix(k_1 \mu - k_2 + k_3)} \right. \\
&\quad \left. - e^{ix(k_1 \mu + k_2 - k_3)} + e^{ix(k_1 \mu - k_2 - k_3)} \right] \\
&= \frac{\pi}{8} \int_{-1}^1 d\mu \left[ \delta^D \left( \mu - \frac{k_2 - k_3}{k_1} \right) + \delta^D \left( \mu + \frac{k_2 - k_3}{k_1} \right) - \right. \\
&\quad \left. \delta^D \left( \mu + \frac{k_2 + k_3}{k_1} \right) - \delta^D \left( \mu - \frac{k_2 + k_3}{k_1} \right) \right]. \tag{C4}
\end{aligned}$$

Here, we have used

$$\begin{aligned}
\sin(k_2 x) \sin(k_3 x) &= \frac{1}{4} \left( e^{ix k_2} e^{ix k_3} - e^{ix k_3} e^{-ix k_2} \right. \\
&\quad \left. - e^{ix k_2} e^{-ix k_3} + e^{-ix k_2} e^{-ix k_3} \right). \tag{C5}
\end{aligned}$$

Once we consider the triangular condition, and that  $k_1 \geq k_2 \geq k_3$ , we obtain

$$V_B = 8\pi^2 k_1 k_2 k_3 (\Delta k)^3 \times \begin{cases} 1 & \text{normal triangles} \\ 1 - \Theta_0 & \text{if } k_1 = k_2 + k_3 \\ \Theta_0 & \text{if } k_2 = k_1 + k_3 \text{ or} \\ & k_3 = k_1 + k_2 \end{cases} \tag{C6}$$

where  $\Theta$  is the Heaviside theta function, and  $\Theta_0 = \frac{1}{2}$ .

#### APPENDIX D: DERIVATION OF THE BISPECTRUM DISTANCE DERIVATES

To calculate the Fisher matrix for the angular diameter distance and the Hubble rate, we need to calculate derivatives of the bispectrum with respect to the distances, namely,  $\frac{\partial B(k_1, k_2, k_3, \mu_1, \mu_2, \mu_3)}{\partial \ln(D_A)}$  and  $\frac{\partial B(k_1, k_2, k_3, \mu_1, \mu_2, \mu_3)}{\partial \ln(H)}$ . However, we are dealing with the variables  $k_1, k_2, k_3, \mu_1, \mu_2$  and  $\mu_3$ , which are not all independent of one another. Hence we perform the chain rule with respect to the independent functions,  $k_1, k_2, k_3(\theta_{12}, \mu_1, \phi), \mu_1, \mu_2(\mu_1, \phi)$ , and  $\mu_3(k_1, k_2, \theta_{12}, \mu_1, \phi)$ . Here, we have written the dependent variables,  $k_3, \mu_2$  and  $\mu_3$ , as functions of the independent variables  $k_1, k_2, \theta_{12}, \mu_1$  and  $\phi$ , which fully describe the shape and orientation of the bispectrum triangles.

Performing the chain rule,

$$\begin{aligned}
\frac{\partial B}{\partial \ln(D_A)} &= \frac{\partial B}{\partial k_1} \frac{\partial k_1}{\partial \ln k_1} \frac{\partial \ln k_1}{\partial \ln(D_A)} + \frac{\partial B}{\partial k_2} \frac{\partial k_2}{\partial \ln k_2} \frac{\partial \ln k_2}{\partial \ln(D_A)} \\
&+ \frac{\partial B}{\partial k_3} \frac{\partial k_3}{\partial \ln k_3} \frac{\partial \ln k_3}{\partial \ln(D_A)} + \frac{\partial B}{\partial \mu_1} \frac{\partial \mu_1}{\partial \ln(D_A)} \\
&+ \frac{\partial B}{\partial \mu_2} \frac{\partial \mu_2}{\partial \ln(D_A)} + \frac{\partial B}{\partial \mu_3} \frac{\partial \mu_3}{\partial \ln(D_A)}, \tag{D1}
\end{aligned}$$

and

$$\begin{aligned}
\frac{\partial B}{\partial \ln(H)} &= \frac{\partial B}{\partial k_1} \frac{\partial k_1}{\partial \ln k_1} \frac{\partial \ln k_1}{\partial \ln(H)} + \frac{\partial B}{\partial k_2} \frac{\partial k_2}{\partial \ln k_2} \frac{\partial \ln k_2}{\partial \ln(H)} \\
&+ \frac{\partial B}{\partial k_3} \frac{\partial k_3}{\partial \ln k_3} \frac{\partial \ln k_3}{\partial \ln(H)} + \frac{\partial B}{\partial \mu_1} \frac{\partial \mu_1}{\partial \ln(H)} \\
&+ \frac{\partial B}{\partial \mu_2} \frac{\partial \mu_2}{\partial \ln(H)} + \frac{\partial B}{\partial \mu_3} \frac{\partial \mu_3}{\partial \ln(H)}, \tag{D2}
\end{aligned}$$

where for notational convenience we have dropped the dependant variables on all functions. For the determination of the actual derivatives, in the evaluation of the second-order kernels, we write  $k_{12} = k_3, k_{13} = k_2$ , and  $k_{23} = k_1$ ; and  $\mu_{12} = -\mu_3, \mu_{13} = -\mu_2$ , and  $\mu_{23} = -\mu_1$ . Following this we find, for example

$$\frac{\partial k_{12}}{\partial k_1} = \frac{\partial k_3}{\partial k_1} = 0, \quad \frac{\partial k_{13}}{\partial k_1} = 0 \quad \text{and} \quad \frac{\partial k_{23}}{\partial k_1} = 1. \tag{D3}$$

We apply similar logic when calculating the derivatives with respect to  $k_2$  and  $k_3$  as well as when performing the derivatives with respect to  $\mu_1, \mu_2$ , and  $\mu_3$ .

When performing the derivatives of the bispectrum with respect to, e.g.,  $k_1$ , we hold  $k_2, k_3, \mu_1, \mu_2$  and  $\mu_3$  fixed, despite  $k_3$  and  $\mu_3$  depending on  $k_1$  as per the definition of the chain rule. We have chosen to write Equations D1 and D2 in the form above, to then insert the following derivatives of  $k_i$  and  $\mu_i$  from Shoji et al. (2009),

$$\frac{\partial \ln k_i}{\partial \ln(D_A)} = 1 - \mu_i^2, \tag{D4}$$

$$\frac{\partial \ln k_i}{\partial \ln(H)} = -\mu_i^2, \tag{D5}$$

$$\frac{\partial \mu_i}{\partial \ln(D_A)} = -\mu_i(1 - \mu_i^2), \tag{D6}$$

and

$$\frac{\partial \mu_i}{\partial \ln(H)} = -\mu_i(1 - \mu_i^2). \tag{D7}$$

#### APPENDIX E: GENERATION OF THE N-DIMENSIONAL LIKELIHOODS

In Section 3 we use the the Fisher matrix to compute the one and two-dimensional likelihoods marginalizing over the remaining parameters in a model of size  $n$ . In a similar way one can compute  $N$ -dimensional likelihoods marginalizing over  $n - N$  parameters:

$$\begin{aligned}
& \mathcal{L}(\mathbf{x}_1, \mathbf{x}_2, \dots, \mathbf{x}_N) \tag{E1} \\
&= \exp \left\{ -\frac{1}{2} \left[ \sum_{i=1}^N \bar{x}_i^2 \left( F_{ii} - \sum_{k,l \neq i}^{n-N} F_{ik} (\bar{F}_{kl})^{-1} F_{li} \right) \right. \right. \\
&\quad \left. \left. + 2 \sum_{j>i}^N \bar{x}_i \bar{x}_j \left( F_{ij} - \sum_{k,l \neq i,j}^{n-N} F_{ik} (\bar{F}_{kl})^{-1} F_{lj} \right) \right] \right\}. \tag{E2}
\end{aligned}$$